Excess-Path-Length Distribution of Fast Charged Particles and Its Relating Problems

中塚，隆郎

(Degree)
博士（理学）
(Date of Degree)
1988-03-18
(Date of Publication)
2008-07-17
(Resource Type)
doctoral thesis
(Report Number)
乙1153
(URL)
https://hdl.handle.net/20.500.14094/D2001153

神　戸　大　学　博　士　論　文

EXCESS-PATH-LENGTH DISTRIBUTION OF FAST CHARGED PARTICLES AND ITS RELATING PROBLEMS

（荷電粒子の径路長の分布及び関連する諸問題）

昭　和　６３　年　１　月

中　塚　隆　郎

EXCESS-PATH-LENGTH DISTRIBUTION OF FAST CHARGED PARTICLES AND ITS RELATING PROBLEMS

Takao Nakatsuka
Department of Physics, Kobe University, Kobe

CONTENTS

SUMMARIES

The Yang equation of the excess-path-length distribution of fast charged particles due to multiple Coulomb scattering under general conditions is completely solved. The solution is an improvement of the Fermi solution, giving the joint distribution of only the angular and the lateral spreads, to include the excess-path-length distribution. The distributions are indicated in figures, and the mean values and the variances of them are tabulated. Effect of a single scattering on the excess-path-length distribution is also investigated using the Molière theory. Influence of the distribution upon the width of other related distributions is found important; e.g. the distribution gives correction about four times more on the width of the energy-loss distribution than on the most probable energy loss. The effect is confirmed in many experimental data.

I. INTRODUCTION

Many detailed investigations have been accumulated on the angular and the lateral distribution of fast charged particles due to multiple Coulomb scattering.[1] But the excess-path-length distribution in the process has not been clearly understood.

Yang proposed a diffusion equation for the excess-path-length distribution of charged particles under the small-angle and the Gaussian approximations.[2] The Yang equation was an advance on the Fermi formulation of the multiple-scattering theory[3] which is a simple and clear diffusion equation to give the joint distribution of the angular and the lateral spreads of the Williams type.[4] Yang derived the excess-path-length distributions of normally incident electrons irrespective of the deflection angle $\vec{\theta}$ and the lateral displacement $\vec{r}$ at emergence (defined as case I by Yang), and with $\vec{\theta}$ fixed at zero and $\vec{r}$ integrated (case II). Scott also dealt with a similar equation. He obtained the solution for the projected excess-path-length distribution corresponding to case II (Ref. 5). But no other work with general solutions followed after Scott and Yang.

Some previous workers discussed and evaluated effects of the average excess path length by using Yang's result on various problems, such as the most probable energy loss[6-9] or the average range[10] of fast charged particles travelling through matter. And another worker limited the step lengths of track in his Monte Carlo calculation of electron-photon showers, using Yang's result,[11] so that the approximations used in the calculation should not provide serious errors. But the corrections by including the excess of path length on those problems were small, within a few percent, because the ratio of the average excess path length to the thickness of the material was so small, as can be evaluated by one-half the average square deflection angle, $\frac{1}{2}[\int<\theta^2>dt]/t$, according to the method of Yang.[2]

The excess-path-length distribution, however, makes its effects on the width in various distributions of those charged particles having passed through a common thickness. An example of such problems is the shape and the width of the energy-loss distribution of fast charged particles in matter. Although it is mainly determined by the statistical fluctuation of collision losses predicted essentially by Landau,[12-16] it receives an additive correction from the excess-path-length distribution.[8,17-20] A correction factor due to the excess-path-length distribution is about four times greater for the width of the energy-loss distribution than for the most probable energy loss, as discussed in the chapter IV. Many experimental results of the energy-loss distribution were compared with the Landau distribution.[18,21-32] Among them, some results having a wider width of energy-loss distribution than the Landau theory could be attributed to the effect of the multiple scattering,[8,26] but a thorough investigation of the effect could not be done because of the insufficiency of applicable theories for experiments of limited geometries.[20] The range distribution[33] of charged particles has a similar problem, having the biggest influence from the residual energy distribution, but requiring corrections for the multiple-scattering detours.[9,34]

Another important example is the arrival time distribution of electron-photon showers developing in the atmosphere, although single particle problems are mainly discussed and shower problems are not much discussed in this paper. As all the shower particles run almost with the velocity of light, the excess-path-length distribution folded over many successive paths is observed as the arrival time distribution of shower particles. The magnitude of the time spread is a few nanoseconds near the shower core, and a few microseconds far from the core.[35] The arrival time distribution is one of the representative observables of an extensive air-shower experiment and the mechanism mentioned above was pointed out in an early report by the MIT group.[36] The accurate calculation, however, has not been done yet due to the difficulty of the scattering theory.[37] If we obtain the excess-path-length distribution function with boundary conditions general enough to pursue electrons in the shower, we can derive the arrival time distribution of the shower particles by the Monte Carlo method.[38,39]

Analytical solutions of the excess-path-length distribution derived by Yang so far were also used to check and evaluate results obtained by a numerical method[40] or a Monte Carlo method[9] for more complicated problems.

Thus, the excess-path-length distribution is very important in a total understanding of the behavior of charged particles in matter. So we searched for the solution of the Yang equation for various conditions, one by one, following the Yang method and obtained the solution of the most general condition. The obtained distributions of excess path length are with $\vec{\theta}$

TABLE I. The conditions for various cases of excess-path-length distributions.

case		correlation	
	$\vec{\theta}_0$	$\vec{\theta}$	$\vec{r}$
I	0	integrated	integrated
II	0	0	integrated
III	0	integrated	0
IV	0	$\vec{\theta}$	integrated
V	0	integrated	$\vec{r}$
gen	$\vec{\theta}_0$	$\vec{\theta}$	$\vec{r}$

integrated and $\vec{r}$ fixed at zero (case III), with $\vec{\theta}$ fixed and $\vec{r}$ integrated (case IV), with $\vec{\theta}$ integrated and $\vec{r}$ fixed (case V), and with $\vec{\theta}$, $\vec{r}$, and the incident angle $\vec{\theta}_0$ fixed (case gen), as indicated in Table I.

Although solutions under the Gaussian approximation are complete in the mathematical sense, they have defects, and have limits in their applications because they only take account of the pure multiple-scattering process. So many authors improved the theory by adding both the single and the plural scattering processes to the multiple-scattering process and examined the effect of including these processes on the angular distributions.[1] We included the single and the plural scattering effects in the equation of the excess-path-length distribution by taking account of the representative Molière theory,[41,42] and obtained the solutions up to the second term in case I and case II. The effects of single scattering and limits of the Gaussian approximation in the path length problem are also discussed in the chapter III.

Effect of the excess-path-length distribution on the energy-loss distribution of fast charged particles is investigated in many experimental data in the chapter IV.

II. THE YANG EQUATION OF THE EXCESS-PATH-LENGTH DISTRIBUTION OF FAST CHARGED PARTICLES

1. Solutions of the Yang Equation

Charged particles traversing through a material of thickness t undergo multiple Coulomb scatterings and change their directions of motion $\vec{\theta}$ successively, so that they receive lateral displacement $\vec{r}$ and the excess of path length Δ:

$$d\vec{r} = \vec{\theta}dt \quad \text{and} \quad d\Delta = (\sec\theta-1)dt = \tfrac{1}{2}\theta^2 dt \tag{1.1}$$

in the small-angle approximation, where we take the t axis along the thickness of the material and the y and the z axes orthogonal to the t axis, all in units of the radiation length[3] and we define the deflection angle $\vec{\theta}$ by the projected vector of direction in the y-z plane, (θ_y, θ_z) in elements. Then the excess path lengths of the projected track in the t-y and the t-z planes, Δ_y and Δ_z, respectively (defined as the projected excess path lengths), are related to the spatial excess path length Δ by

$$d\Delta_y + d\Delta_z = \tfrac{1}{2}(\theta_y^2+\theta_z^2)dt = d\Delta. \tag{1.2}$$

The problem is to obtain the correlated probability density of charged particles, having passed t_0 with $\vec{\theta}_0$, $\vec{r}_0$, and $\vec{\Delta}_0$, and having reached t with $\vec{\theta}$, $\vec{r}$, and $\vec{\Delta}$ (Ref. 43), in the most general condition, $P(t,\vec{\theta},\vec{r},\vec{\Delta},t_0,\vec{\theta}_0,\vec{r}_0,\vec{\Delta}_0)d\vec{\theta}d\vec{r}d\vec{\Delta}$, in the form of a Green's function. We obtain the distributions according to Yang's method.[44]

Under the Gaussian approximation, scattering is independent in y and z components, so P can be represented as the product of distributions for projected components in the t-y and the t-z planes:

$$P = F(t, \theta_y, y, \Delta_y, t_0, \theta_{y0}, y_0, \Delta_{y0}) F(t, \theta_z, z, \Delta_z, t_0, \theta_{z0}, z_0, \Delta_{z0}). \quad (1.3)$$

The diffusion equation proposed by Yang for the projected components is

$$\frac{\partial F}{\partial t} + \theta\frac{\partial F}{\partial y} - \frac{1}{w^2}\frac{\partial^2 F}{\partial \theta^2} + \frac{1}{2}\theta^2\frac{\partial F}{\partial \Delta} = \delta(t-t_0)\delta(\theta-\theta_0)\delta(y-y_0)\delta(\Delta-\Delta_0), \quad (1.4)$$

where

$$w = 2pv/E_s \quad (1.5)$$

and E_s is the scattering energy defined by Rossi and Greisen.[3] Because of the translational invariance of Eq. (1.4) with respect to t, y, and Δ, we see they will appear in the solution in the form of $t-t_0$, $y-y_0$, and $\Delta-\Delta_0$, so we can put zeroes into t_0, y_0, and Δ_0, temporarily.

Applying the Fourier transforms with y and the Laplace transforms with Δ

$$F = \frac{1}{4\pi^2 i}\int d\lambda e^{\Delta\lambda}\int e^{iy\eta}\psi(t, \theta, \eta, \lambda, \theta_0) d\eta, \quad (1.6)$$

we can obtain the solution ψ in a form of orthogonal expansion by the eigenfunctions, as Yang did,

$$\psi = w\sqrt{\omega}\exp(-\frac{\eta^2}{2\lambda}t-\omega t)\sum_{n=0}^{\infty}\psi_n(w\sqrt{\omega}(\theta_0+\frac{i\eta}{\lambda}))\psi_n(w\sqrt{\omega}(\theta+\frac{i\eta}{\lambda}))e^{-2n\omega t}, \quad (1.7)$$

where

$$\psi_n(x) = (\sqrt{\pi}2^n n!)^{-\frac{1}{2}}H_n(x)\exp(-\frac{1}{2}x^2) \quad \text{and} \quad \lambda = 2w^2\omega^2, \quad (1.8)$$

and $H_n(x)$ and $He_n(x)$, appearing later, are both Hermite polynomials.[4,5]

The series (1.7) must be summed before we apply the inverse Laplace transforms. Yang derived the sums only for the case that the variables in ψ_n's are both zero, when the series is reduced to the binomial one (cases I and II). To get the solutions for other conditions, the series of greater generality must be summed. By using the generalized generating function of the eigenfunctions,

$$\sum_{n=0}^{\infty}\psi_n(x)\psi_n(y)z^n = \frac{1}{\sqrt{\pi}\sqrt{1-z^2}}\exp\left[-\frac{(x^2+y^2)(1+z^2)-4xyz}{2(1-z^2)}\right] \qquad (1.9)$$

as proved in Appendix A. The sum corresponding to the most general condition is

$$\psi = (2\pi \,\mathrm{sh}\sqrt{s})^{-\frac{1}{2}} w\sqrt{\omega}\exp\left[-\frac{\eta^2}{2\lambda}t\right.$$

$$\left.-\frac{w^2\omega}{2\,\mathrm{sh}\sqrt{s}}\{(\theta^2+\theta_0^2)\mathrm{ch}\sqrt{s}-2\theta\theta_0+[\frac{2i\eta}{\lambda}(\theta+\theta_0)-\frac{2\eta^2}{\lambda^2}](\mathrm{ch}\sqrt{s}-1)\}\right], \qquad (1.10)$$

where we have abbreviated sinh, cosh, and tanh with sh, ch, and th, respectively, and have introduced a new complex variable

$$s = 4t^2\omega^2 = 2t^2\lambda/w^2. \qquad (1.11)$$

Applying the inverse Fourier transforms against η we obtain

$$\xi d\phi d\rho = \frac{d\phi d\rho}{\pi}\frac{s}{\sqrt{3(2-2\mathrm{ch}\sqrt{s}+\sqrt{s}\,\mathrm{sh}\sqrt{s})}}\exp\left[-\frac{s^2}{3(2-2\mathrm{ch}\sqrt{s}+\sqrt{s}\,\mathrm{sh}\sqrt{s})}\right.$$

$$\times\{\frac{\mathrm{sh}\sqrt{s}}{\sqrt{s}}\rho^2-\frac{2\sqrt{3}}{s}(\mathrm{ch}\sqrt{s}-1)\rho(\phi+\phi_0)+3s^{-\frac{3}{2}}(\sqrt{s}\,\mathrm{ch}\sqrt{s}-\mathrm{sh}\sqrt{s})(\phi^2+\phi_0^2)$$

$$\left.-6s^{-\frac{3}{2}}(\sqrt{s}-\mathrm{sh}\sqrt{s})\phi\phi_0\}\right], \qquad (1.12)$$

where we used nondimensional variables for the deflection angle and the lateral displacement of the track by dividing by their spatial root mean squares at a thickness t predicted under the Gaussian approximation:

$$\vec{\phi} = \vec{\theta}/\langle\theta^2\rangle_{av}^{\frac{1}{2}}, \qquad \vec{\rho} = \vec{r}/\langle r^2\rangle_{av}^{\frac{1}{2}}, \qquad (1.13)$$

and

$$\langle\theta^2\rangle_{av} = 4t/w^2, \qquad \langle r^2\rangle_{av} = \tfrac{4}{3}t^3/w^2. \qquad (1.14)$$

The probability density for the projected components are obtained by the inverse Laplace transforms against λ. If we change the integral variable from λ to s and introduce the new nondimensional variable

$$u = \tfrac{1}{2}w^2\Delta/t^2 \qquad (1.15)$$

as defined by Yang (a factor of $\frac{1}{4}$ is multiplied into the Yang definition for a slight simplification of expressions), then we have

$$F d\theta dy d\Delta = \frac{d\phi d\rho du}{2\pi i}\int_{s_0-i\infty}^{s_0+i\infty} e^{us}\xi(\phi,\rho,s,\phi_0)ds, \qquad (1.16)$$

where the path of integration is taken parallel to the imaginary axis, in the half-plane of convergence of ξ. It should be noted that t does not appear explicitly after we used the nondimensional variables, ϕ, ρ, and u.

The joint distribution for the spatial excess path length, $A_{gen}(t,\vec{\theta},\vec{r},\Delta,\vec{\theta}_0)d\vec{\theta}d\vec{r}d\Delta$, can be obtained using the folding property of the Laplace transforms. Then

$$A(t,\vec{\theta},\vec{r},\Delta,\vec{\theta}_0)d\vec{\theta}d\vec{r}d\Delta = B(\vec{\phi},\vec{\rho},u,\vec{\phi}_0)d\vec{\phi}d\vec{\rho}du$$

$$= \frac{d\vec{\phi}d\vec{\rho}du}{2\pi i}\int e^{us}\Xi(\vec{\phi},\vec{\rho},s,\vec{\phi}_0)ds, \qquad (1.17)$$

where

$$\Xi(\vec{\phi},\vec{\rho},s,\vec{\phi}_0) = \xi(\phi_y,\rho_y,s,\phi_{0y})\xi(\phi_z,\rho_z,s,\phi_{0z}). \qquad (1.18)$$

The distributions corresponding to other situations, from cases I–V, can be obtained by integrating the joint distribution with respect to $\vec{\theta}$ and/or $\vec{r}$ or substituting zero into them. The Laplace transformed solutions for the spatial excess path length so obtained are tabulated in Table II together with their abscissas of convergence, where we introduced new variables

$$\vec{\phi}' = \vec{\phi}-\vec{\phi}_0 \quad \text{and} \quad \vec{\rho}' = \vec{\rho}-\sqrt{3}\vec{\phi}_0. \qquad (1.19)$$

TABLE II. Laplace-transformed distributions of the spatial excess path length and their abscissas of convergence. The results of Yang and Scott (case I and II) are listed together. μ is the smallest positive solution satisfying $\mu = \tan\mu$.

CASE	LAPLACE TRANSFORMED DISTRIBUTION	ABSCISSA OF CONVERGENCE
I	$\frac{1}{\mathrm{ch}\sqrt{s}}$	$-\frac{1}{4}\pi^2$
II	$\frac{d\vec{\phi}}{\pi}\frac{\sqrt{s}}{\mathrm{sh}\sqrt{s}}$	$-\pi^2$
III	$\frac{d\vec{\rho}}{3\pi}\frac{s^{3/2}}{\sqrt{s}\,\mathrm{ch}\sqrt{s}-\mathrm{sh}\sqrt{s}}$	$-\mu^2$
IV	$\frac{d\vec{\phi}}{\pi}\frac{\sqrt{s}}{\mathrm{sh}\sqrt{s}}\exp[-\sqrt{s}\,\phi^2\coth\sqrt{s}]$	$-\pi^2$
V	$\frac{d\vec{\rho}}{3\pi}\frac{s^{3/2}}{\sqrt{s}\,\mathrm{ch}\sqrt{s}-\mathrm{sh}\sqrt{s}}\exp[-\frac{\rho^2}{3}\frac{s^{3/2}\mathrm{ch}\sqrt{s}}{\sqrt{s}\,\mathrm{ch}\sqrt{s}-\mathrm{sh}\sqrt{s}}]$	$-\mu^2$
gen	$\frac{d\vec{\phi}d\vec{\rho}}{\pi^2}\frac{s^2/3}{2-2\mathrm{ch}\sqrt{s}+\sqrt{s}\,\mathrm{sh}\sqrt{s}}\exp[-\frac{s^2/3}{2-2\mathrm{ch}\sqrt{s}+\sqrt{s}\,\mathrm{sh}\sqrt{s}}$	
	$\times\{3\frac{\sqrt{s}\,\mathrm{ch}\sqrt{s}-\mathrm{sh}\sqrt{s}}{s^{3/2}}\phi'^2-2\sqrt{3}\,\frac{\mathrm{ch}\sqrt{s}-1}{s}(\vec{\phi}\vec{\rho}'+\vec{\phi}_0\vec{\rho})+\frac{\mathrm{sh}\sqrt{s}}{\sqrt{s}}\rho^2\}]$	$-4\pi^2$

2. Calculation of the Distributions and the Moments

The distributions for the spatial excess path length and their moments will be derived in this section. The results for cases I and II are already given in Yang's original paper.

For case III only those particles with an arbitrary angle and r=0 at an emergence are detected. Then

$$\Xi_{III}(s)\,d\vec{\rho}$$

$$= \frac{d\vec{\rho}}{3\pi}\,\frac{s^{3/2}}{\sqrt{s}\,\mathrm{ch}\sqrt{s}-\mathrm{sh}\sqrt{s}}$$

$$= \frac{2d\vec{\rho}}{3\pi}\left[\frac{1}{\sqrt{s}-1}s^{\frac{3}{2}}e^{-\sqrt{s}}-\left(\frac{1}{\sqrt{s}-1}+\frac{2}{(\sqrt{s}-1)^2}\right)s^{\frac{3}{2}}e^{-3\sqrt{s}}+\ \ldots\ldots\right], \tag{2.1}$$

hence

$$B_{III}(u)\,d\vec{\rho}du$$

$$= \frac{2d\vec{\rho}du}{3\pi}\Big[\frac{1}{\sqrt{\pi u}}\left(\frac{1}{8u^3}-\frac{1}{2u^2}+1\right)\exp\left(-\frac{1}{4u}\right)+e^{u-1}\,\mathrm{erfc}\left(\frac{1}{2\sqrt{u}}-\sqrt{u}\right)$$

$$-\frac{\sqrt{u}}{\sqrt{\pi}}\left(\frac{27}{8u^4}+\frac{9}{2u^3}+\frac{6}{u^2}+\frac{7}{u}+4\right)\exp\left(-\frac{9}{4u}\right)-4u+3)\,e^{u-3}\,\mathrm{erfc}\left(\frac{3}{2\sqrt{u}}-\sqrt{u}\right)$$

$$+\ \ldots\ldots\Big]. \tag{2.2}$$

By taking the asymptotic approximation derived from the first term of the alternating series, good to within 1 %,

$$B_{III}(u)$$

$$= \frac{2}{3\pi}\left\{\frac{1}{\sqrt{\pi u}}\left(\frac{1}{8u^3}-\frac{1}{2u^2}+1\right)\exp\left(-\frac{1}{4u}\right)+e^{u-1}\,\mathrm{erfc}\left(\frac{1}{2\sqrt{u}}-\sqrt{u}\right)\right\} \quad \text{for } u\leq 0.2,$$

$$= \frac{2}{3\pi}\,\frac{-\mu^2}{\cos\mu}e^{-\mu^2 u} \quad \text{for } u\geq 0.2, \tag{2.3}$$

where μ=4.493... is defined by the smallest positive solution of the transcendental equation

$$\mu = \tan\mu, \tag{2.4}$$

and $-\mu^2$ is the abscissa of convergence for case III.

In cases IV, V, and gen, the inverse Laplace transforms conducted in the preceding cases are difficult to apply due to the existence of essential singularities, so we will apply the saddle-point method, which is less accurate but yields a fairly good result for the image functions with rapidly increasing values along the real axis.

Generally, in this method, we can approximate the complex integral at the saddle point $\bar{s}$, appearing on the real axis at the right-hand side of the abscissa of convergence; thus

$$B(u) = \frac{1}{2\pi i}\int e^{us}\Xi(s)\,ds = \left(2\pi\frac{\partial^2}{\partial s^2}\ln\Xi(\bar{s})\right)^{-\frac{1}{2}}\Xi(\bar{s})e^{u\bar{s}}, \qquad (2.5)$$

with

$$u = -\frac{\partial}{\partial s}\ln\Xi(\bar{s}). \qquad (2.6)$$

It should be noted that $\sqrt{s}$, $\mathrm{sh}\sqrt{s}$, and $\mathrm{ch}\sqrt{s}$ are replaced by $i\sqrt{-s}$, $i\sin\sqrt{-s}$, and $\cos\sqrt{-s}$ when s takes negative values. The accuracy of the method in the general case is discussed by Nishimura.[46] The difference of the result obtained by this method for case I from the accurate one is shown in Fig. 1. The discrepancy between them is within a few percent.

The logarithmic derivatives are used in this method. As an example, the explicit calculation for case V is shown in Appendix B.

The Fermi solution should be derived by integrating our solution B(u) over the excess path length (zeroth moment), or by taking the limiting value of $\Xi(s)$ at $s\to0$:

$$\lim_{s\to0}\Xi_{gen} = \frac{4}{\pi^2}\exp[-4\{\phi'^2-\sqrt{3}\vec{\phi}'\cdot\vec{\rho}'+\rho'^2\}], \qquad (2.7)$$

which agree with the Fermi solution indicated by Scott[47] where the nondimensional incident angle ϕ_0 is not fixed at zero.

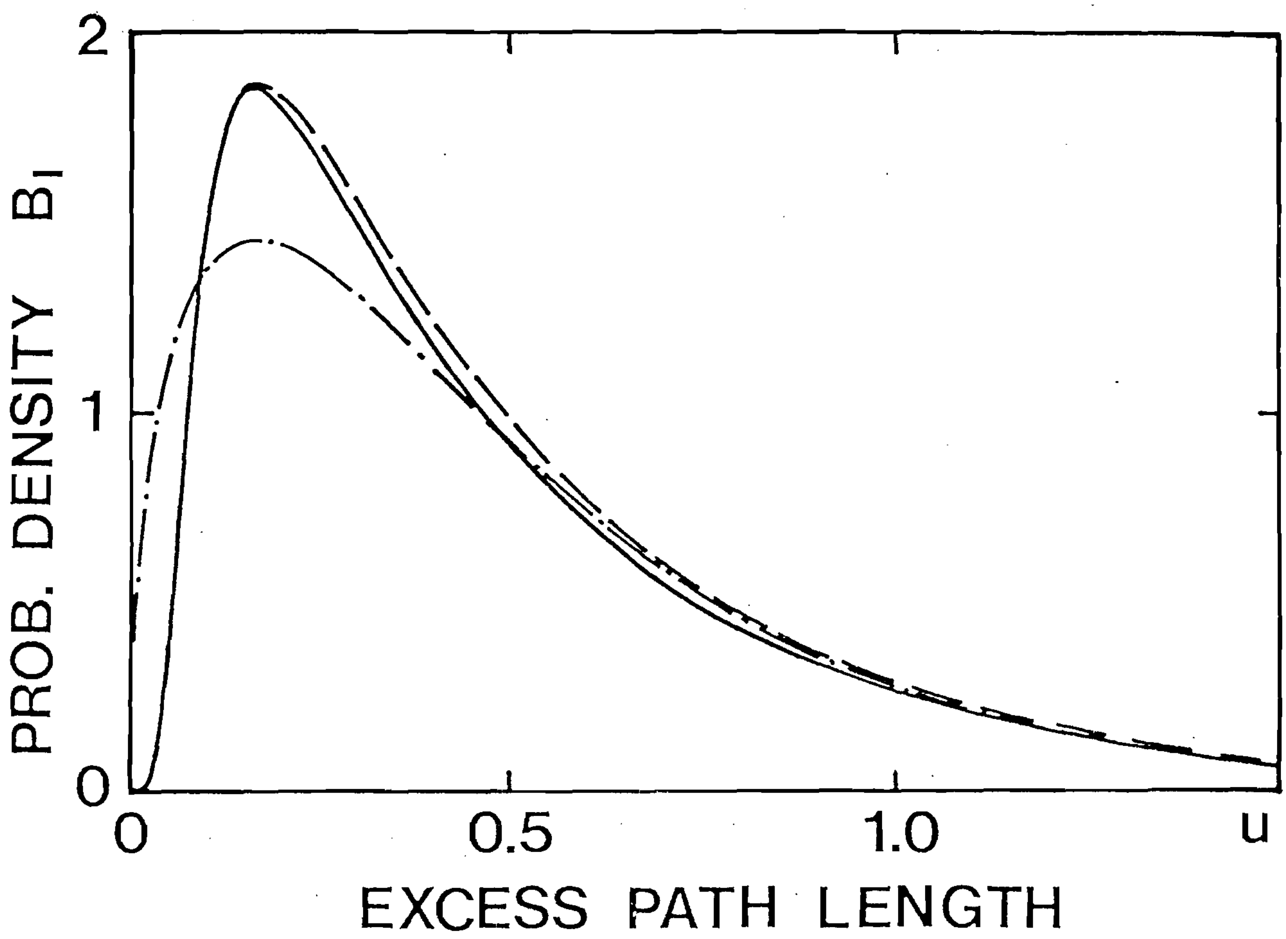

Fig. 1. Comparison of the solution for case I obtained by the saddle-point method (dashed curve) and the exact results (solid curve). Gamma distribution of the same mean value and variance is also compared (dot-dashed curve). Abscissa u is nondimensional spatial excess path length defined by (1.15) in the text.

Mean values and variances are easily calculated from the limit of $s\to 0$ of the first and the second logarithmic derivatives of Ξ,

$$\langle u\rangle_{av} = -\lim_{s\to 0}\frac{\partial}{\partial s}\ln\Xi(s) \tag{2.8}$$

and

$$\langle u^2\rangle_{av}-\langle u\rangle_{av}^2 = \lim_{s\to 0}\frac{\partial^2}{\partial s^2}\ln\Xi(s), \tag{2.9}$$

and are shown in Table III (Ref. 48). The table contains the Bichsel and Uehling results of mean excess path length for case III and $\vec{\vartheta}=\vec{r}=0$ (Ref. 10) as special cases. One characteristic feature is that the mean excess path length of cases IV, V, and gen at a deflection angle and a lateral displacement of covariant values, $\langle\phi^2\rangle_{av}=\langle\rho^2\rangle_{av}=1$ and $\langle\vec{\phi}\vec{\rho}\rangle_{av}=\sqrt{3}/2$, agree with that of case I.

3. Characteristic Features of the Excess-Path-Length Distribution

We will discuss characteristic features of the excess-path-length distributions in this section.

The peak position u_p of case I can be evaluated from the first term of Yang's expansion, Eq. (13) of Ref. 2; thus,

$$u_p = \tfrac{1}{6} \qquad \text{and} \qquad B_I(u=\tfrac{1}{6}) = 1.85, \tag{3.1}$$

within an accuracy of 0.015 %. The positions at the half-peak value are determined numerically as u_H = 0.0727 and 0.4954; thus the full width at the half-height is

$$\Gamma_u = 0.423. \tag{3.2}$$

$B_I(u)$ is compared in Fig. 1 with the gamma distribution[45] of the same mean and variance:

$$G(u) = \frac{6}{\sqrt{\pi}}\,(3u)^{\frac{1}{2}}e^{-3u}. \tag{3.3}$$

TABLE III. Mean and variance of the excess-path-length distributions.

CASE	MEAN	VARIANCE
I	$\frac{1}{2}$	$\frac{1}{6}$
II, IV	$\frac{1}{6}+\frac{1}{3}\phi^2$	$\frac{1}{90}+\frac{2}{45}\phi^2$
III, V	$\frac{1}{10}+\frac{2}{5}\rho^2$	$\frac{1}{350}+\frac{2}{525}\rho^2$
gen	$\frac{1}{15}+\frac{2\phi'^2-\sqrt{3}(\vec{\phi}\vec{\rho}'+\vec{\phi}_0\vec{\rho})+6\rho^2}{15}$	$\frac{11}{12600}+\frac{11\phi'^2-3\sqrt{3}(\vec{\phi}\vec{\rho}'+\vec{\phi}_0\vec{\rho})+3\rho^2}{3150}$

The latter has the peak value 1.45 at $u = \frac{1}{6}$, and the full width at the half-height of 0.598. So, B_I starts more slowly near u=0 but increases more rapidly, and reaches the peak at almost the same position with a greater peak value, and decreases more slowly as $\exp(-\frac{1}{4}\pi^2 u)$ after the peak. B_I has the narrower full width at the half-height than the gamma distribution.

According to Symon,[13] the relative width of the range fluctuation of electrons is

$$<(r-\bar{r})^2>_{av}^{\frac{1}{2}} / \bar{r} \sim \text{several ten percent.} \qquad (3.4)$$

On the other hand, the relative width of the path length distribution to the thickness evaluated from Table III for case I is

$$<(R-\bar{R})^2>_{av}^{\frac{1}{2}} / \bar{R} \sim \sqrt{\tfrac{1}{6}}\,\frac{2}{w^2}\bar{R}. \qquad (3.5)$$

Thus for an electron with kinetic energy E of the order of E_s^2/ε or less, (3.4) and (3.5) become comparable if we assume its mean energy to be E/2 and the mean range to be E/ε, although in this problem the loss of the energy of the traversing particle should not be neglected in the theory.

The excess-path-length distributions at a fixed deflection angle integrated over the lateral displacement (cases II and IV) are shown in Fig. 2. The area under the curve, which gives the probability density against $d\vec{\phi}$, is $\pi^{-1}\exp(-\phi^2)$. As the deflection angle increases, the peak position and the mean value of excess path length increases (Table III). In this case, the distribution starts from u=0 and the width of the distribution increases rapidly with the angle.

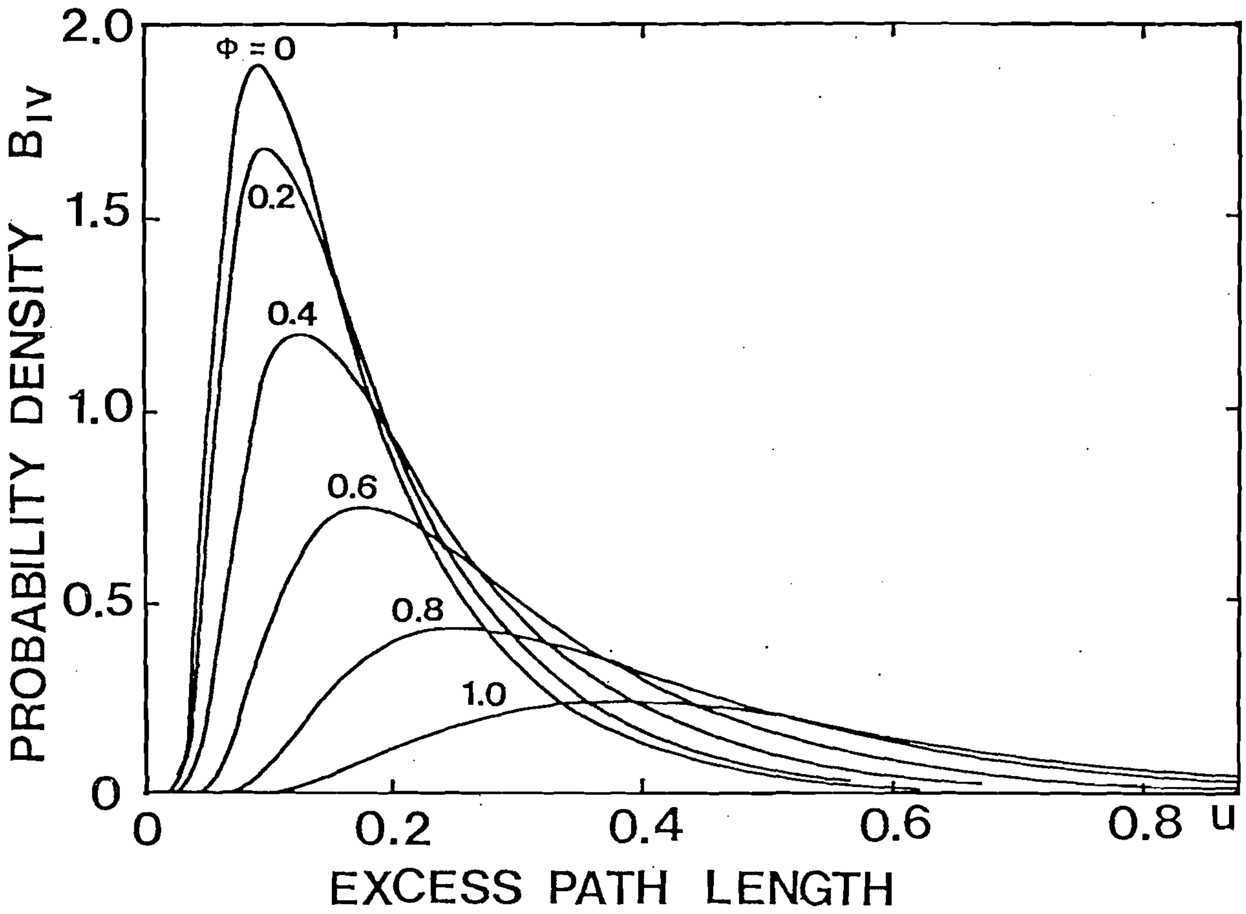

Fig. 2. Path-length distributions of a fast charged particle with its deflection angle fixed and lateral displacement integrated (cases II and IV). The parameter in the figure represents the deflection angle in the unit of the spatial root mean square, defined by (1.13) in the text.

The distribution at a fixed lateral displacement integrated over the deflection angle (cases III and V) is shown in Fig. 3. The area under the distribution curve is $\pi^{-1}\exp(-\rho^2)$. As the lateral displacement increases, the mean and the width of the excess-path-length distribution also increase. But in this case the smallest excess path length u_θ (denoted as the geometrical excess) exists due to a difference between the chord length[5] of track and the thickness of the material. In the small-angle approximation, it is estimated as

$$u_\theta = \frac{w^2}{2t^2}(\sqrt{t^2+r^2}-t) = \frac{w^2 r^2}{4t^3} = \frac{1}{3}\rho^2, \qquad (3.6)$$

which agrees with the limiting value of our solution of (2.6) at $\bar{s}\to\infty$:

$$\lim_{\bar{s}\to\infty} B = 0 \quad \text{as} \quad \lim_{\bar{s}\to\infty} u = \frac{1}{3}\rho^2 = u_\theta. \qquad (3.7)$$

Thus the mean excess path length of case V is composed of two parts; the geometrical excess u_θ and the pure multiple-scattering excess u_s defined as

$$u_s \equiv \langle u_V\rangle_{av} - u_\theta = \frac{1}{10} + \frac{1}{15}\rho^2. \qquad (3.8)$$

At a lateral displacement of $\rho=1$, the pure multiple-scattering excess is a half of the geometrical excess. At a smaller distance the fraction of the pure multiple-scattering excess becomes dominant and at a larger distance that of the geometrical excess becomes dominant in the actual excess.

The Monte Carlo calculation of the time structure of electron-photon showers by Locci, Picchi and Verri[49] underestimated the electron detours because it took account of only the geometrical excess using the Molière distribution,[41] and

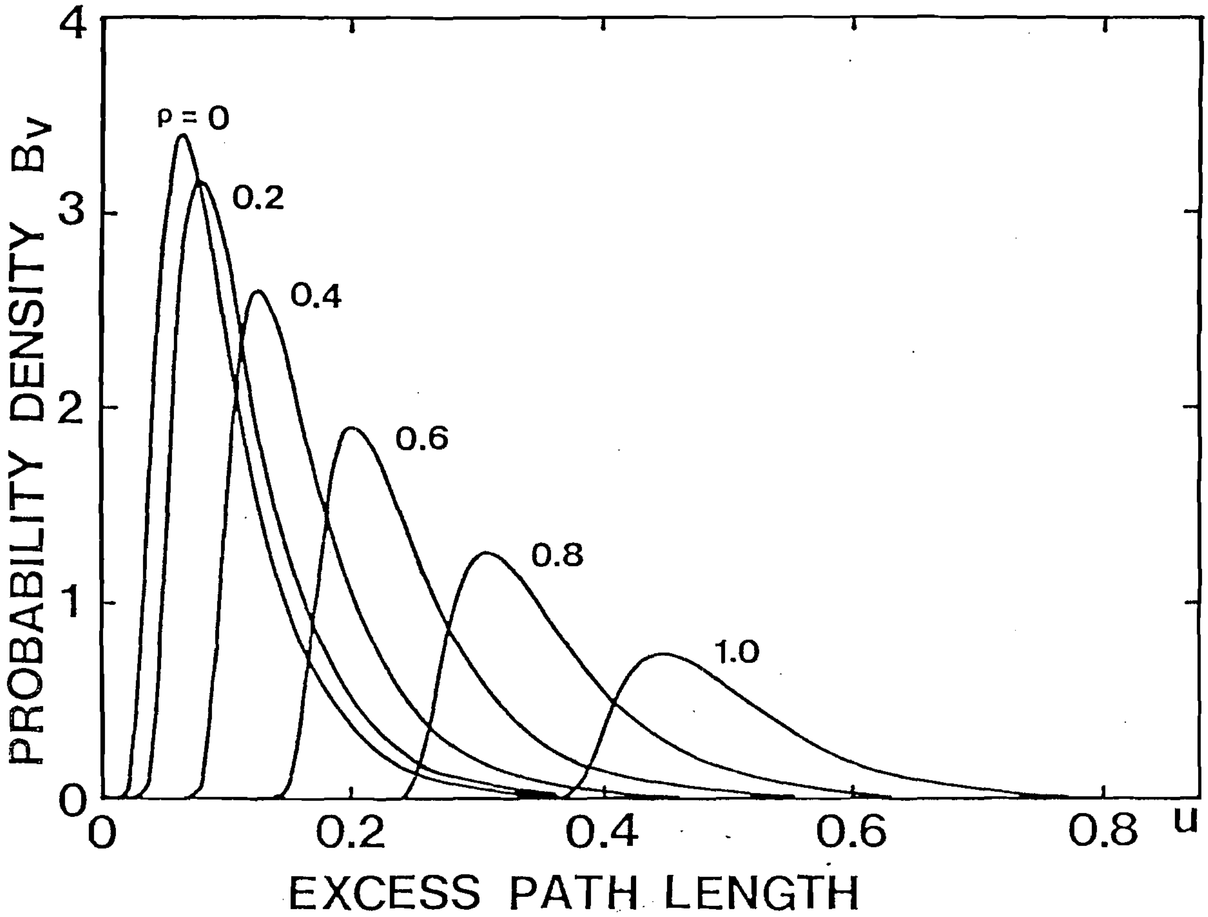

Fig. 3. Path-length distributions of a fast charged particle with its deflection angle integrated and lateral displacement fixed (cases III and V). The parameter in the figure represents the lateral displacement in the unit of the spatial root mean square, defined by (1.13) in the text.

the calculation by Baxter[50] gave the narrow width of the distribution because it only took account of the average excess path length.

The distribution at a fixed deflection angle and a fixed lateral displacement (case gen) is shown in Fig. 4. The area under the distribution curve is $4\pi^{-2}\exp[-4(\phi'^2-\sqrt{3}\vec{\phi}'\vec{\rho}'+\rho'^2)]$, as shown in (2.7). Thus with $\phi=1$, for example as in the figure, it becomes maximum at $\rho=\sqrt{3}/2$. As angle between $\vec{\phi}$ and $\vec{\rho}$ in the y-z plane increases, the area decreases and the mean excess and the width of the distribution increases, reflecting a longer detour of the path. The smallest excess path length, $u_0=\rho^2/3$, is also determined by the geometrical excess.

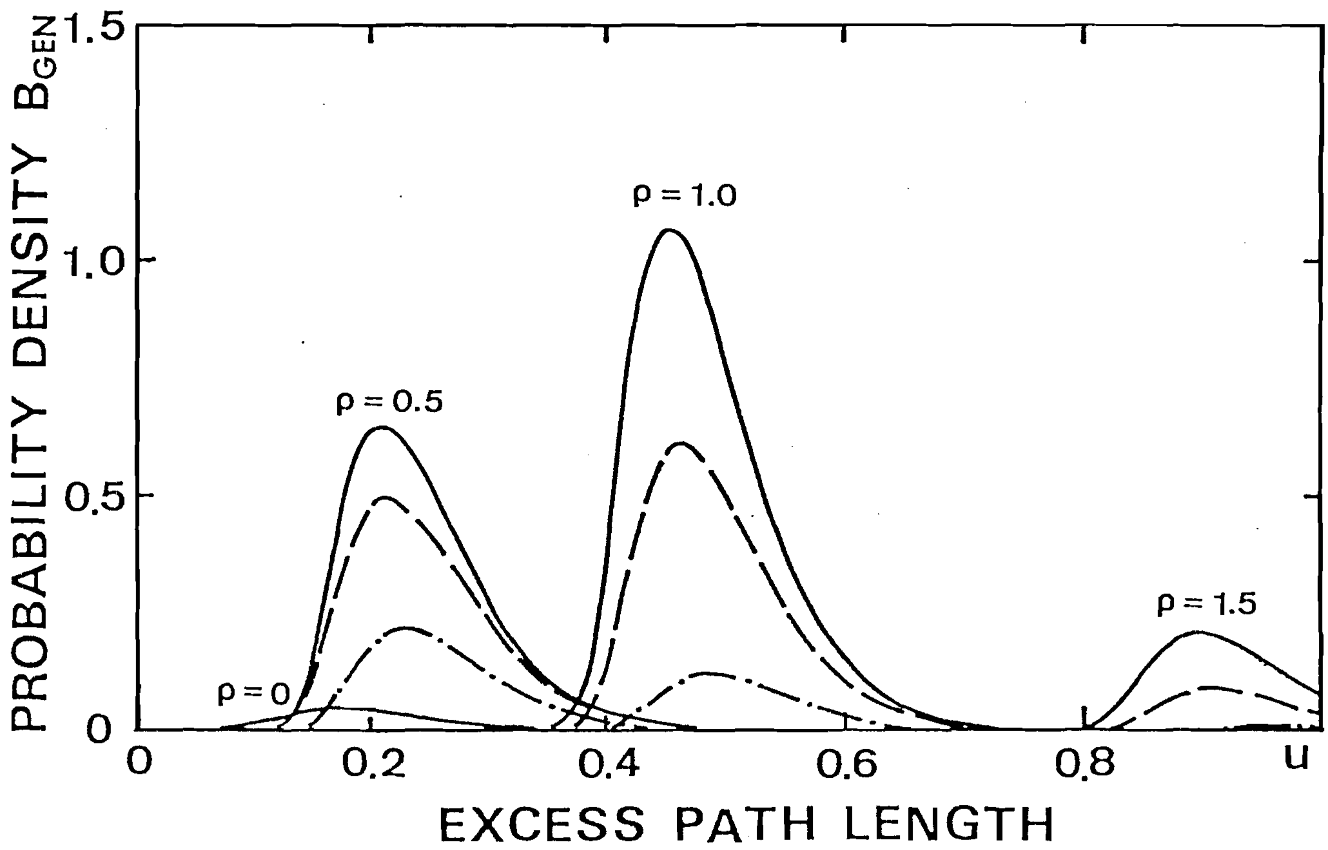

Fig. 4. Path-length distributions of a fast charged particle with its deflection angle and lateral displacement, which are both in the y-z plane, fixed (case gen). In the figure the angles of incidence are all zero, $\phi_0=0$, the deflection angles at at emergence are all taken as 1 ($|\vec{\vartheta}|=1$), the lateral displacements ρ are distinguished by the parameter in the figure, and the angles between the vectors $\vec{\vartheta}$ and $\vec{\rho}$ are taken as 0 (solid curve), $\frac{1}{8}\pi$ (dashed curve) and $\frac{1}{4}\pi$ (dot-dashed curve), respectively.

III. THE EXCESS-PATH-LENGTH DISTRIBUTION OF FAST CHARGED PARTICLES CONSIDERING THE SINGLE SCATTERING

4. Excess-Path-Length Distribution under the Molière theory

The Gaussian approximation assumes the lower and the higher cuts, θ_{min} and θ_{max}, on the Rutherford cross section and requires vanishing of the fourth and the higher moments with respect to the nondimensional angle ϕ, or

$$\phi_{max} = w\theta_{max}/(2\sqrt{t}) \ll 1. \qquad (4.1)$$

Equation (4.1) however corresponds to a long path length, say $t \gg 25$ as indicated in Appendix C, so at an ordinary thickness the tail of cross section at large angles strongly influences the angular distribution. Thus the single and the plural scatterings should be taken into account in the theory. Molière included the single and plural scattering probabilities in his multiple-scattering theory by regarding θ_{max} infinite. So he assumed only the lower cut of the cross section corresponding to the screening potential of the Thomas-Fermi potential, and evaluated it as $\sqrt{e}\chi_a$ by the WKB method.[42,51]

The excess-path-length distribution under the Molière theory can be solved for cases I and II using the Kamata and Nishimura formulation[46,52] indicated in Appendix D.

Let $A(t,\vec{\theta},\Delta)d\vec{\theta}d\Delta$ denote the correlated probability density between the spatial excess path length and the direction of motion, with the lateral displacement integrated. The diffusion equation is

$$\frac{\partial A}{\partial t} - \iint [A(\vec{\theta}-\vec{\theta}') - A(\vec{\theta})]\,\sigma(\vec{\theta}')\,d\vec{\theta}' + \frac{1}{2}\theta^2\frac{\partial A}{\partial \Delta} = 0. \qquad (4.2)$$

The Laplace transforms with Δ and the Fourier transforms with $\vec{\theta}$ are

$$\bar{A}(t,\vec{\theta},\lambda) = \int_0^\infty e^{-\lambda\Delta} A(t,\vec{\theta},\Delta)\,d\Delta \tag{4.3}$$

and

$$\tilde{A}(t,\vec{\zeta},\lambda) = \iint e^{-i\vec{\theta}\vec{\zeta}} \bar{A}(t,\vec{\theta},\lambda)\,d\vec{\theta}. \tag{4.4}$$

Then the transformed diffusion equation for (4.2) becomes

$$\frac{\partial\tilde{A}}{\partial t} + \frac{\zeta^2\tilde{A}}{w'^2} - \frac{\lambda}{2}\left(\frac{\partial^2}{\partial\zeta_y^2} + \frac{\partial^2}{\partial\zeta_z^2}\right)\tilde{A} = \frac{1}{\Omega}\frac{\zeta^2}{w'^2}\tilde{A}\ln\frac{\zeta^2}{w'^2}, \tag{4.5}$$

where the additive term characteristic to the Kamata and Nishimura formulation appears at the right-hand side, and w' is defined by

$$w' = 2pv/K, \tag{4.6}$$

and K is a constant defined by Kamata and Nishimura.[46,52]

If we expand the solution in a power series as

$$\tilde{A}(t,\vec{\zeta},\lambda) = \tilde{A}^{(0)}(t,\vec{\zeta},\lambda) + \frac{1}{\Omega}\tilde{A}^{(1)}(t,\vec{\zeta},\lambda) + \ldots\ , \tag{4.7}$$

the recurrence equations are obtained (hereafter we abbreviate w' with w):

$$\begin{aligned}\left[\frac{\partial}{\partial t} + \frac{\zeta^2}{w^2} - \frac{\lambda}{2}\left(\frac{\partial^2}{\partial\zeta_y^2} + \frac{\partial^2}{\partial\zeta_z^2}\right)\right]\tilde{A}^{(n)} &= \frac{\zeta^2}{w^2}\tilde{A}^{(n-1)}\ln\frac{\zeta^2}{w^2} && \text{for } n>0,\\ &= \delta(t) && \text{for } n=0.\end{aligned} \tag{4.8}$$

This is a linear differential equation equivalent to the Yang equation of case IV, with a known inhomogenious term in the right-hand side. As we see in (4.8), the first term of series (4.7) gives the solutions of the Yang equation.

We can solve this equation using the Green's function defined by

$$[\frac{\partial}{\partial t} + \frac{\zeta^2}{w^2} - \frac{\lambda}{2}(\frac{\partial^2}{\partial\zeta_y{}^2} + \frac{\partial^2}{\partial\zeta_z{}^2})]\tilde{G}(t, \vec{\zeta}, t', \vec{\zeta}') = \delta(t-t')\delta^2(\vec{\zeta}-\vec{\zeta}'). \qquad (4.9)$$

The explicit form of the Green's function is obtained by the same mathematical method indicated in the Sec. 1:

$$\tilde{G}(t, \vec{\zeta}, t', \vec{\zeta}')$$

$$= \frac{1}{2\pi w^2 \omega \mathrm{sh}(2\omega(t-t'))}$$

$$\times \exp[-\frac{\zeta^2+\zeta'^2}{2w^2\omega}\coth(2\omega(t-t')) + \frac{\vec{\zeta}\vec{\zeta}'}{w^2\omega \mathrm{sh}(2\omega(t-t'))}]. \qquad (4.10)$$

The incident angle of zero corresponds to the uniform distribution with $\vec{\zeta}'$ at $t'=0$, so the first term $\tilde{A}^{(0)}(t, \vec{\zeta}, \lambda)$ becomes

$$\tilde{A}^{(0)}(t, \vec{\zeta}, \lambda) = \iint d\vec{\zeta}' \tilde{G}(t, \vec{\zeta}, 0, \vec{\zeta}')$$

$$= \frac{1}{\mathrm{ch}(2\omega t)} \exp[-\frac{\zeta^2}{2w^2\omega}\mathrm{th}(2\omega t)], \qquad (4.11)$$

and the subsequent terms can be obtained from

$$\tilde{A}^{(n)}(t, \vec{\zeta}, \lambda)$$

$$= \int_0^t dt' \iint d\zeta' \tilde{G}(t, \vec{\zeta}, t', \vec{\zeta}')\tilde{A}^{(n-1)}(t', \vec{\zeta}', \lambda)\frac{\zeta'^2}{w^2}\ln\frac{\zeta'^2}{w^2}. \qquad (4.12)$$

A. Case I

The Laplace transformed distribution is obtained by substituting $\vec{\zeta}=0$ in (4.11) and (4.12). Using the complex variable s, the first term becomes

$$\tilde{A}^{(0)}(t, \vec{\zeta}=0, \lambda) = \frac{1}{\mathrm{ch}\sqrt{s}} \equiv \Xi_I{}^{(0)}(s), \qquad (4.13)$$

which agrees with the Yang solution, and the second term becomes

$$\tilde{A}^{(1)}(t, \vec{\zeta}=0, \lambda)$$

$$= \int_0^t dt' \iint d\vec{\zeta}' \frac{1}{2\pi w^2 \omega \mathrm{sh}(2\omega(t-t'))} \exp[-\frac{\zeta'^2}{2w^2\omega}\coth(2\omega(t-t'))]$$

$$\times \frac{1}{ch(2\omega t')} \exp[-\frac{\zeta'^2}{2w^2\omega} th(2\omega t')] \frac{\zeta'^2}{w^2} \ln\frac{\zeta'^2}{w^2}$$

$$= -\frac{\ln(ch\sqrt{s})}{2ch\sqrt{s}} + \frac{\sqrt{s}sh\sqrt{s}}{2ch^2\sqrt{s}}\{1-\gamma+\ln\frac{s}{tch\sqrt{s}} + \frac{1}{\sqrt{s}}\int_0^{\sqrt{s}} \ln\frac{shxchx}{x}dx\}$$

$$\equiv \Xi_{I}^{(1)}(t,s), \tag{4.14}$$

where $\gamma=0.5772...$ is Euler's constant. Inverse Laplace transforms from $\Xi(s)$ to $B(u)$ will be obtained in the next section.

B. Case II

Applying the inverse Fourier transforms with $\vec{\zeta}$ for (4.11) and (4.12) and setting $\vec{\theta}=0$, the Laplace transformed distribution for case II is obtained. The first term agrees with the Yang solution

$$\bar{A}^{(0)}(t,\vec{\theta}=0,\lambda)d\vec{\theta} = \frac{1}{\pi}\frac{\sqrt{s}}{sh\sqrt{s}}d\vec{\phi} \equiv \Xi_{II}^{(0)}(s)d\vec{\phi}, \tag{4.15}$$

and the second term becomes

$$\bar{A}^{(1)}(t,\vec{\theta}=0,\lambda)d\vec{\theta}$$

$$= \frac{d\vec{\theta}}{4\pi^2}\int_0^t dt' \iint d\vec{\zeta}' \frac{1}{ch(2\omega(t-t'))} \exp[-\frac{\zeta'^2}{2w^2\omega} th(2\omega(t-t'))]$$

$$\times \frac{1}{ch(2\omega t')} \exp[-\frac{\zeta'^2}{2w^2\omega} th(2\omega t')] \frac{\zeta'^2}{w^2} \ln\frac{\zeta'^2}{w^2}$$

$$= [\frac{\sqrt{s}sh\sqrt{s}+sch\sqrt{s}}{2\pi sh^2\sqrt{s}}(-\gamma+\ln\frac{\sqrt{s}}{tsh\sqrt{s}}) + \frac{sch\sqrt{s}}{\pi sh^2\sqrt{s}}\{1+\frac{1}{\sqrt{s}}\int_0^{\sqrt{s}}\ln(chx)dx\}]d\vec{\phi}$$

$$\equiv \Xi_{II}^{(1)}(t,s)d\vec{\phi}. \tag{4.16}$$

5. The correction Term of the Distribution by the Molière Theory

Applying the inverse Laplace transforms against λ, the excess-path-length distributions are obtained. The first terms $B^{(0)}$'s are the solutions of the Yang equation themselves. So we will obtain in this section the second terms $B^{(1)}$'s and their asymptotic forms for large excess path length, in cases I and II.

A. Case I

From (4.14)

$$\Xi_I^{(1)}(t,s) = (\ln\sqrt{s}+1-\gamma-\ln(2t))\sqrt{s}e^{-\sqrt{s}}+(\ln 2-\frac{\pi^2}{24})e^{-\sqrt{s}}$$

$$-\ 3(\ln\sqrt{s}+2-\gamma-\ln(2t))\sqrt{s}e^{-3\sqrt{s}}-(1+\ln 2-\frac{\pi^2}{8})e^{-3\sqrt{s}}$$

$$+\ \ldots\ . \tag{5.1}$$

Using the formulae with the inverse Laplace transforms,[45]

$$L^{-1}[s^{\frac{1}{2}(n-1)}e^{-k\sqrt{s}}] = 2^{-n}(\pi u^{n+1})^{-\frac{1}{2}}H_n(\frac{k}{2\sqrt{u}})\exp(-\frac{k^2}{4u}) \tag{5.2}$$

and

$$L^{-1}[s^{\frac{1}{2}n-1}e^{-k\sqrt{s}}\ln\sqrt{s}]$$

$$= -\frac{\sqrt{2}}{\sqrt{\pi}}(2u)^{-\frac{1}{2}(n+1)}\int_k^\infty\{\gamma+\ln(x-k)\}He_n(\frac{x}{\sqrt{2u}})\exp(-\frac{x^2}{4u})dx, \tag{5.3}$$

we obtain the series of rapid convergence in the small u region:

$$B_I^{(1)}(t,u)$$

$$=L^{-1}[\sqrt{s}e^{-\sqrt{s}}\ln\sqrt{s}]+\frac{1}{4}\{(1-\gamma-\ln(2t))(\frac{1}{u}-2)+2\ln 2-\frac{\pi^2}{12}\}\frac{1}{\sqrt{\pi u^3}}\exp(-\frac{1}{4u})$$

$$-3L^{-1}[\sqrt{s}e^{-3\sqrt{s}}\ln\sqrt{s}]-\frac{3}{4}\{(2-\gamma-\ln(2t))(\frac{9}{u}-2)+2+2\ln 2-\frac{\pi^2}{4}\}\frac{1}{\sqrt{\pi u^3}}\exp(-\frac{9}{4u})$$

$$+\ \ldots\ . \tag{5.4}$$

The terms relevant to (5.3) can be calculated by numerical integrals.

In the large-u region, the contributions from the singularity of s with largest real components give rapid convergence. Equation (4.14) has logarithmic branches at $s=0$, $-(\pi/2)^2$, $-\pi^2$, ..., and poles at $s=-(\pi/2)^2$, $-(3\pi/2)^2$, $-(5\pi/2)^2$, ... Logarithmic branches can be paired as $\ln(s/(s+\frac{1}{4}\pi^2))$, $\ln((s+\frac{1}{4}\pi^2)/(s+\pi^2))$, ..., then we see they contribute analogously as poles. A counterclockwise complex integral around the cut connecting the pair of branches is reduced to a curvilinear integral on the cut:

$$\frac{1}{2\pi i}\int_C f(s)\ln\frac{s-\alpha}{s-\beta}ds$$

$$= \int_\alpha^\beta \{f(s)-\Sigma(\text{principal part at pole on cut})\}ds \qquad (5.5)$$

as proved in Appendix E, which corresponds to the residue in case of pole.

Thus we can develop (4.14) as

$$\Xi_I{}^{(1)}(t,s)$$

$$= -\frac{1}{2ch\sqrt{s}}\ln\frac{ch\sqrt{s}}{s+\frac{1}{4}\pi^2}$$

$$+\frac{\sqrt{s}sh\sqrt{s}}{2ch^2\sqrt{s}}\{-1-\gamma+\ln\frac{s+\frac{1}{4}\pi^2}{tch\sqrt{s}}+\frac{i\pi}{\sqrt{s}}\ln(\frac{\pi}{2}+\frac{\sqrt{s}}{i})+\frac{1}{\sqrt{s}}\int_0^{\sqrt{s}}\ln\frac{shxchx}{x(x+\frac{1}{4}\pi^2)}dx\}$$

$$+\frac{\sqrt{s}sh\sqrt{s}}{2ch^2\sqrt{s}}\ln\frac{s}{s+\frac{1}{4}\pi^2}+\frac{1}{2ch^2\sqrt{s}}\{(\sqrt{s}-\frac{i\pi}{2})sh\sqrt{s}-ch\sqrt{s}\}\ln\frac{s+\frac{1}{4}\pi^2}{s+\pi^2}$$

$$+O(\ln(s+\pi^2)). \qquad (5.6)$$

The first and the second terms only have a pole at $s=-\frac{1}{4}\pi^2$ in the region of $R(s) > -\pi^2$, where R indicates the real part, so

$$B_I{}^{(1)}(t,u)$$

$$= -\frac{\pi}{4}[-5+4\gamma+4\ln t+\pi^2u\{2-\gamma-\ln(2t)\}]e^{-\frac{1}{4}\pi^2u}$$

$$+\int_0^{-\frac{1}{4}\pi^2}[\frac{\sqrt{s}sh\sqrt{s}}{2ch^2\sqrt{s}}e^{us}+\frac{\pi^3\exp(-\frac{1}{4}\pi^2u)}{4(s+\frac{1}{4}\pi^2)^2}\{1+(u-\frac{4}{\pi^2})(s+\frac{1}{4}\pi^2)\}]ds$$

$$+\int_{-\frac{1}{4}\pi^2}^{-\pi^2}\frac{1}{2ch^2\sqrt{s}}\{(\sqrt{s}-\frac{i}{2}\pi)sh\sqrt{s}-ch\sqrt{s}\}e^{us}ds+O(e^{-\pi^2u})$$

$$= \frac{\pi}{4}[6-4\gamma+4\ln\frac{\pi}{8t}-\pi^2u(1-\gamma+\ln\frac{\pi}{16t})]e^{-\frac{1}{4}\pi^2u}$$

$$-\int_0^{-\frac{1}{4}\pi^2}\frac{i}{2\sqrt{s}}\{1+5us+2u^2s^2\}e^{us}\ln\frac{1-ish\sqrt{s}}{1+ish\sqrt{s}}ds$$

$$- \int_{-\frac{1}{4}\pi^2}^{-\pi^2} \{\frac{i}{4\sqrt{s}}+(\frac{3}{4}\pi-\frac{2\sqrt{s}}{i})u+(\frac{\pi}{2}-\frac{\sqrt{s}}{i})u^2 s\} e^{us} \ln\frac{1-i\,sh\sqrt{s}}{1+i\,sh\sqrt{s}}\,ds$$

$$+ O(e^{-\pi^2 u}), \tag{5.7}$$

where we applied partial integrals in order not to drop significant digits in the subtractions.

Series (5.4) for small u and (5.7) for large u agree well within 2 % in the vicinity of u=0.7.

Asymptotic features at u >> 1 are derived from the first term of (5.7). Near s=0,

$$\frac{\sqrt{s}\,sh\sqrt{s}}{2ch^2\sqrt{s}}e^{us} = (\frac{1}{2}s-\frac{5}{12}s^2+\ \ldots\ )e^{us}, \tag{5.8}$$

so

$$B_I{}^{(1)}(t,u) \sim \int_0^{-\frac{1}{4}\pi^2}(\frac{1}{2}s-\frac{5}{12}s^2+\ \ldots\ )e^{us}ds,$$

$$\sim \frac{1}{2u^2}+\frac{5}{6u^3}+\ \ldots\ . \tag{5.9}$$

B. Case II

From (4.16)

$$\Xi_{II}{}^{(1)}(t,s) = \frac{1}{\pi}(1-\gamma+\ln\frac{\sqrt{s}}{2t})\,s e^{-\sqrt{s}} + \frac{1}{\pi}(\frac{\pi^2}{12}-\gamma+\ln\frac{2\sqrt{s}}{t})\sqrt{s}e^{-\sqrt{s}}$$

$$+\frac{3}{\pi}(2-\gamma+\ln\frac{\sqrt{s}}{2t})\,s e^{-3\sqrt{s}} + \frac{1}{\pi}(\frac{\pi^2}{4}-\gamma+\ln\frac{2\sqrt{s}}{t})\sqrt{s}e^{-3\sqrt{s}}$$

$$+\ \ldots\ . \tag{5.10}$$

So in the small-u region

$$B_{II}{}^{(1)}(t,u)$$

$$= \frac{1}{\pi}L^{-1}[(s+\sqrt{s})e^{-\sqrt{s}}\ln\sqrt{s}]$$

$$+\frac{1}{4}\{\frac{1}{u}(1-\gamma-\ln(2t))(\frac{1}{2u}-3)+(\frac{\pi^2}{12}-\gamma+\ln\frac{2}{t})(\frac{1}{u}-2)\}(\pi u)^{-\frac{3}{2}}\exp(-\frac{1}{4u})$$

$$+\ \frac{1}{\pi}L^{-1}[(3s+\sqrt{s})e^{-3\sqrt{s}}\ln\sqrt{s}]$$

$$+\frac{1}{4}\{\frac{9}{u}(2-\gamma-\ln(2t))(\frac{9}{2u}-3)+(\frac{\pi^2}{4}-\gamma+\ln\frac{2}{t})(\frac{9}{u}-2)\}(\pi u)^{-\frac{3}{2}}\exp(-\frac{9}{4u})$$

$$+\ \ldots\ . \tag{5.11}$$

We can develop (4.16) as

$$\Xi_{II}{}^{(1)}(t,s)$$

$$=\frac{\sqrt{s}\,\mathrm{sh}\sqrt{s}+s\,\mathrm{ch}\sqrt{s}}{2\pi\,\mathrm{sh}^2\sqrt{s}}\{-\gamma+\ln\frac{\sqrt{s}(s+\pi^2)}{t\,\mathrm{sh}\sqrt{s}}\}$$

$$+\frac{s\,\mathrm{ch}\sqrt{s}}{\pi\,\mathrm{sh}^2\sqrt{s}}\{-1+\frac{i\pi}{\sqrt{s}}\ln(\frac{\pi}{2}+\frac{\sqrt{s}}{i})+\frac{1}{\sqrt{s}}\int_0^{\sqrt{s}}\ln\frac{\mathrm{ch}x}{x^2+\frac{1}{4}\pi^2}dx\}$$

$$+\frac{2s-i\pi\sqrt{s}}{2\pi\,\mathrm{sh}^2\sqrt{s}}\mathrm{ch}\sqrt{s}\ln\frac{s+\frac{1}{4}\pi^2}{s+\pi^2}+\frac{(s-i\pi\sqrt{s})\,\mathrm{ch}\sqrt{s}-\sqrt{s}\,\mathrm{sh}\sqrt{s}}{2\pi\,\mathrm{sh}^2\sqrt{s}}\ln\frac{s+\pi^2}{s+\frac{9}{4}\pi^2}$$

$$+\ O(\ln(s+\tfrac{9}{4}\pi^2)), \tag{5.12}$$

so in the large-u region we have

$$B_{II}{}^{(1)}(t,u)$$

$$=\ -2\pi e^{-\pi^2 u}\{(\pi^2u-2)(1-\gamma+\ln\frac{\pi}{8t})-2\ln 2\}$$

$$-\frac{1}{\pi}\int_{-\frac{1}{4}\pi^2}^{-\pi^2}\{3-\frac{i\pi}{2\sqrt{s}}+(7-\frac{5i\pi}{2\sqrt{s}})us+(2-\frac{i\pi}{\sqrt{s}})u^2s^2\}e^{us}\ln\frac{1-\mathrm{ch}\sqrt{s}}{1+\mathrm{ch}\sqrt{s}}ds$$

$$-\frac{1}{\pi}\int_{-\pi^2}^{-\frac{9}{4}\pi^2}\{1-\frac{i\pi}{2\sqrt{s}}+(3-\frac{5i\pi}{2\sqrt{s}})us+(1-\frac{i\pi}{\sqrt{s}})u^2s^2\}e^{us}\ln\frac{1-\mathrm{ch}\sqrt{s}}{1+\mathrm{ch}\sqrt{s}}ds$$

$$+\ O(e^{-\frac{9}{4}\pi^2 u}). \tag{5.13}$$

Series (5.11) for small u and (5.13) for large u agree well, within 1 %, in the vicinity of u=0.4.

The asymptotic expansion at u>>1 is

$$B_{II}{}^{(1)}(t,u)\ \sim\ \frac{1}{\pi}\int_{-\frac{1}{4}\pi^2}^{-\pi^2}\frac{s\,\mathrm{ch}\sqrt{s}}{\mathrm{sh}^2\sqrt{s}}(1-\frac{i\pi}{2\sqrt{s}})e^{us}ds$$

$$\sim\ (\frac{1}{\pi^3}u^{-3}+\frac{5\pi^2-6}{2\pi^6}u^{-5}+\ \ldots\ )e^{-\frac{1}{4}\pi^2 u}. \tag{5.14}$$

6. Effect of the Molière Cross Section on the Excess-Path-Length Distribution

The first terms $B^{(0)}$'s are Yang's solutions themselves, only w being replaced by w' or E_s by K. There is no explicit dependence on t in $B^{(0)}$'s after we used the nondimensional variable u. In the second terms $B^{(1)}$'s the dependence on t appears through lnt, reflecting the Kamata and Nishimura formulation. $B^{(0)}(u)$'s and $B^{(1)}(t,u)$'s at t=1 as well as the coefficient of lnt in $B^{(1)}$'s are indicated in Figs. 5 and 6 for cases I and II, respectively.

The corrections by the second term characteristic to the Molière theory are a long tail appearing in the distribution for case I and a slight additional contribution appearing at a small excess path length. They qualitatively agree with the corrections indicated by Molière in the angular distribution (Fig. 7), i.e., the long tail of the distribution at large angles and the slight additional contribution at small angles.

$B^{(1)}(t,u)$ must be weighted by $1/\Omega$. Comparison of the first term and the weighted second term for air (Ω=15.2) at t=1 is indicated in Fig. 8. The distinctive long tail tends to fall as $1/(2\Omega u^2)$ as predicted in (5.9). This tail can be interpreted as the geometrical excess from the single scattering.

In fact, the single scattering at t' yields the geometrical excess of

$$\Delta = \tfrac{1}{2}\theta^2(t-t') \tag{6.1}$$

at t in the small-angle approximation. Its probability is given by the Rutherford cross section:

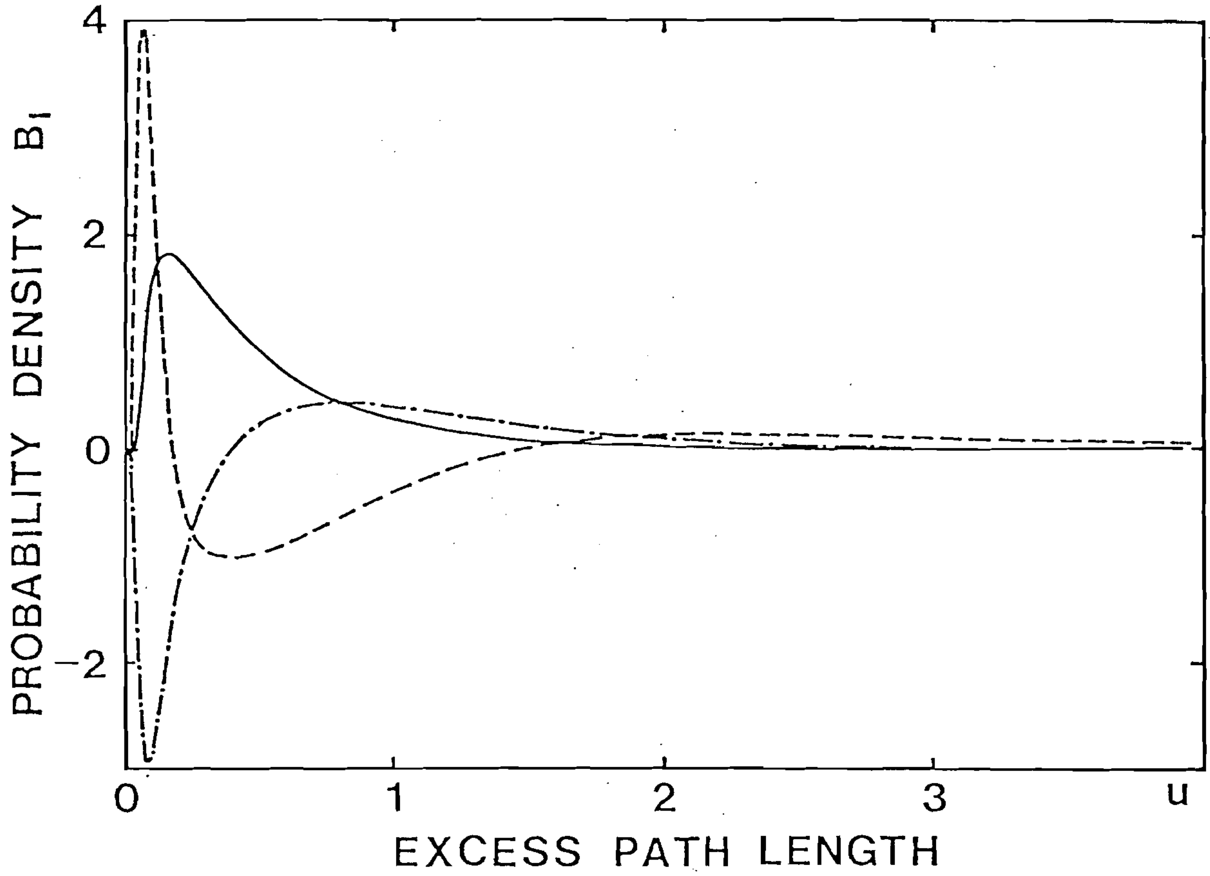

Fig. 5. Path-length distribution in case I under the Molière cross section. The first term $B_I^{(0)}$ (solid curve) and the second term $B_I^{(1)}$ at t=1 (dashed curve) with its coefficient for lnt (dot-dashed curve). The long tail reflecting the single scattering appears in $B_I^{(1)}$.

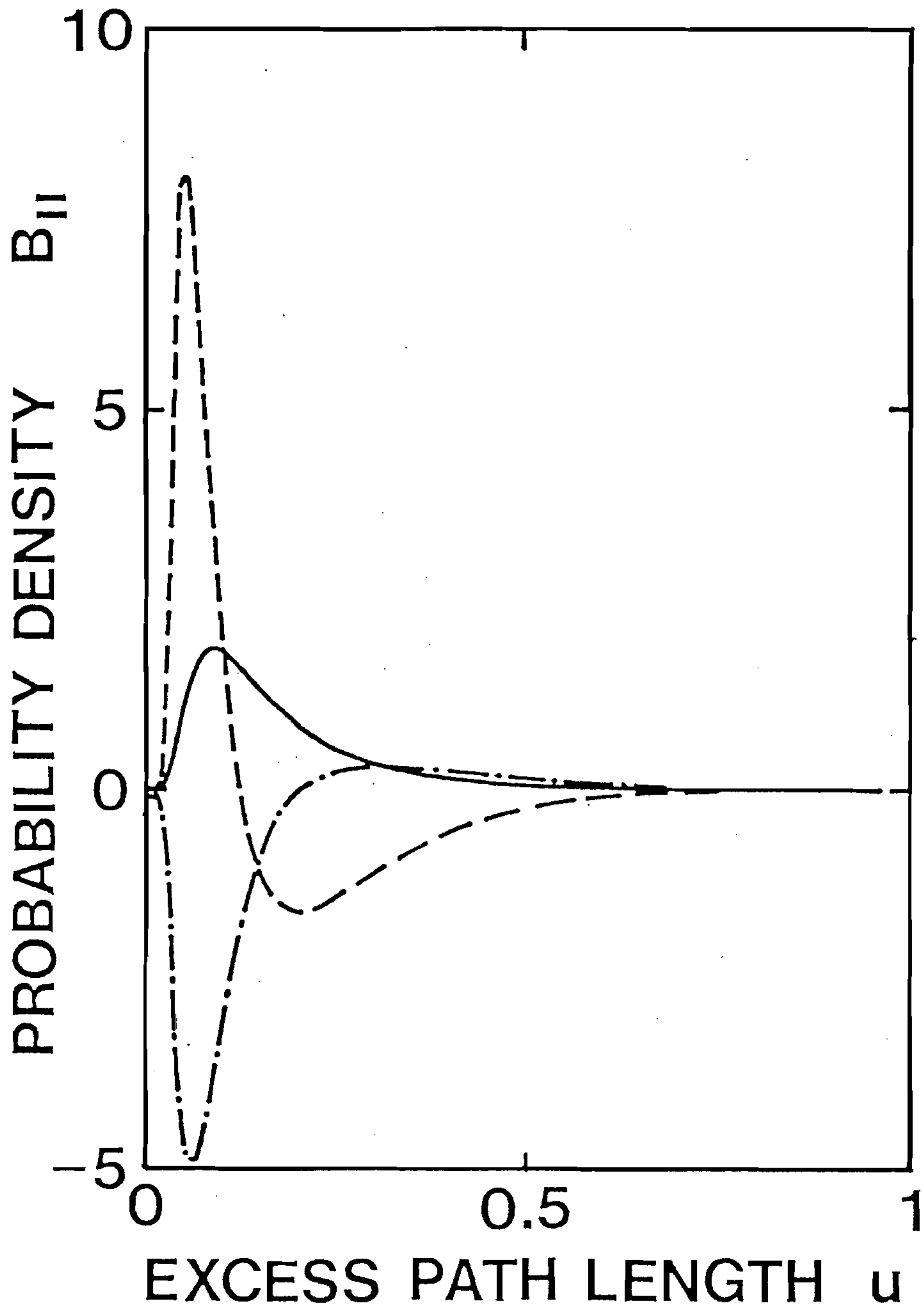

Fig. 6. Path−length distribution in case II under the Molière cross section.

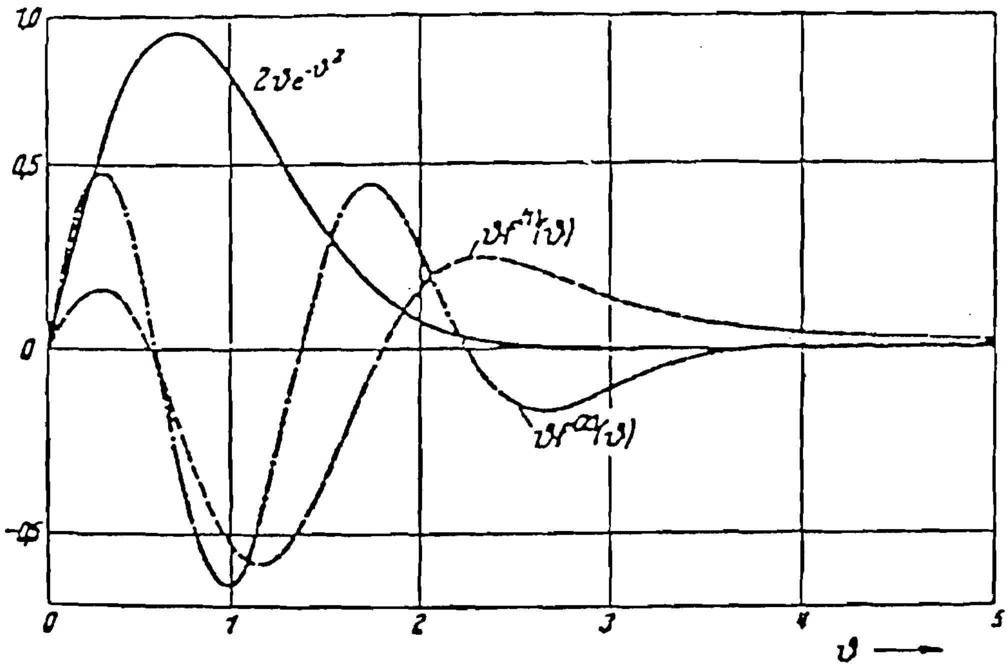

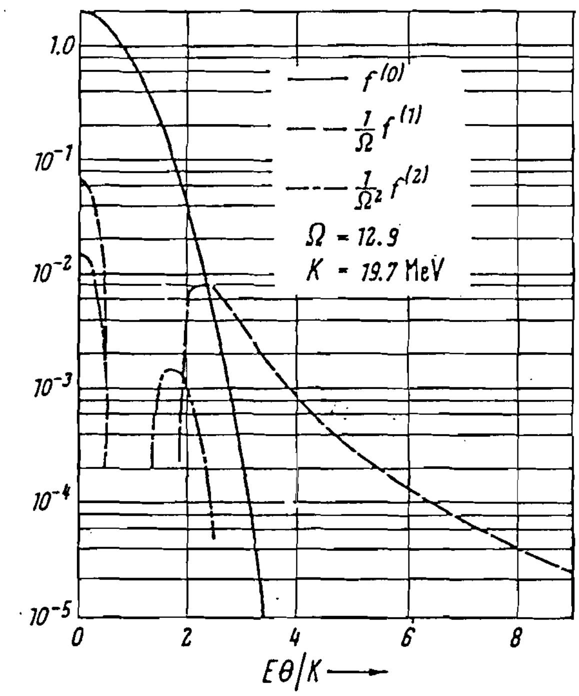

Fig. Contribution of the successive terms to the scattering under the depth of one radiation length in Pb according to MOLIÈRE's theory.

Fig. 7. Correction of the angular distribution of fast charged particles by the Moliere theory. The figures are cited from Refs. 41 and 46.

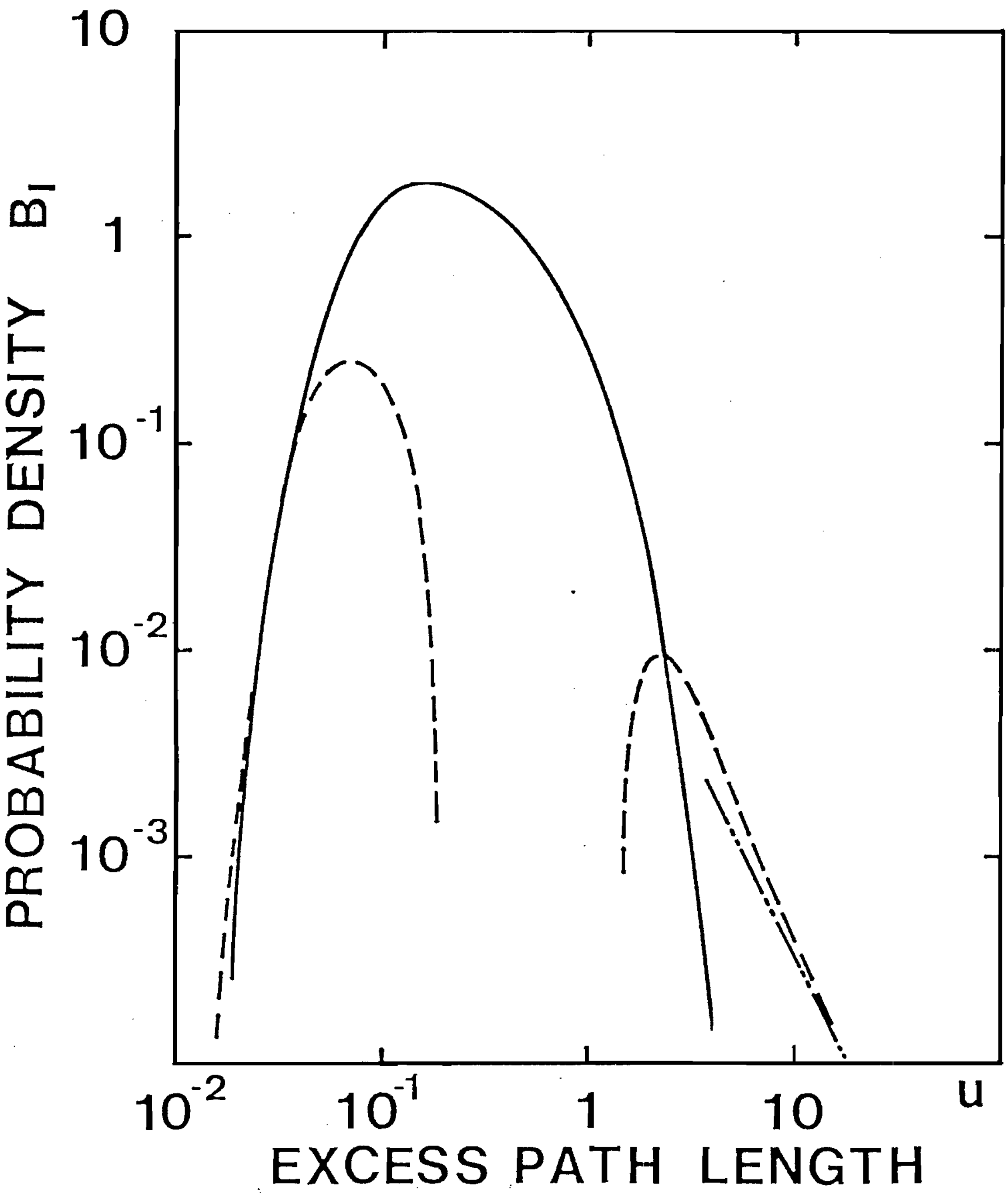

Fig. 8. Comparison between the first term $B_I^{(0)}$ (solid curve) of the distribution in case I and the weighted second term $B_I^{(1)}/\Omega$ at t=1 (dashed curve). The long tail tends to the geometrical excess by the single scattering (double-dot-dashed curve) indicated in (6.3) in the text.

$$\sigma(\theta)2\pi\theta d\theta dx' = \frac{2}{\Omega}\frac{K^2}{p^2v^2}\frac{d\theta}{\theta^3}dt'$$

$$= \frac{2}{\Omega}\frac{K^2}{p^2v^2}\frac{d\Delta}{4\Delta^2}(t-t')dt', \tag{6.2}$$

where we used the constants introduced by Kamata and Nishimura. Integrating (6.2) with t' from 0 to t, we obtain

$$B(u)du = \frac{1}{\Omega}\frac{K^2}{p^2v^2}\frac{t^2}{4\Delta^2}d\Delta = \frac{1}{\Omega}\frac{du}{2u^2}. \tag{6.3}$$

This interpretation, attributing to the geometrical excess is reinforced by the fact that we see no distinctive tail other than the exponential fall in case II.

IV. EFFECT OF THE EXCESS-PATH-LENGTH DISTRIBUTION ON THE STRAGGLING PROBLEM

7. The Landau Distribution of Energy Loss for the Fast Charged Particles

Charged particles traversing through materials lose their energy due to collisions with atomic electrons. The mean dissipating rate of energy is about 2.5 $MeV \cdot g^{-1} cm^2$ for fast charged articles.[53] But the actual value of energy loss against a certain length of passage is not constant but receives statistical fluctuation. This problem is called straggling. Landau predicted the form of the fluctuation.

Let $f(x, \Delta_E) d\Delta_E$ be the differential probability for fast charged particles to lose their energy of Δ_E after the passage of length x. The diffusion equation proposed by Landau is[12]

$$\frac{\partial f}{\partial x} = \int_0^\infty W(\varepsilon) [f(x, \Delta_E - \varepsilon) - f(x, \Delta_E)] d\varepsilon, \tag{7.1}$$

where W(E) denotes the probability density to lose energy of E in a single scattering;[54]

$$W(E) = \frac{2\pi N e^4 \rho \Sigma Z}{m v^2 \Sigma A} \frac{1}{E^2}, \tag{7.2}$$

where ΣZ and ΣA are the sums of the atomic number and the atomic weight of the substance, respectively.

According to Landau, the solution of Eq. (7.1) is

$$f(x, \Delta_E) d\Delta_E = \frac{d\Delta_E}{\xi} \phi(\lambda), \tag{7.3}$$

where

$$\phi(\lambda) = \frac{1}{2\pi i} \int_{\sigma - i\infty}^{\sigma + i\infty} e^{u \ln u + \lambda u} du, \tag{7.4}$$

and

$$\lambda = \frac{1}{\xi}[\Delta_E - \xi(\ln\frac{\xi}{\varepsilon'} + 1 - \gamma)]. \tag{7.5}$$

ξ in Eqs. (7.3) and (7.5) is a measure of the thickness[12] proportional to x, with the dimension of energy, expressed as

$$\xi = x\frac{2\pi Ne^4\rho\Sigma Z}{mv^2\Sigma A}, \tag{7.6}$$

ε' is defined as

$$\ln\varepsilon' = \ln\frac{(1-v^2/c^2)I^2}{2mv^2} + \frac{v^2}{c^2}, \tag{7.7}$$

where I is an ionization energy of the atom, and γ denotes Euler's constant. $\phi(\lambda)$ becomes maximum at $\lambda=-0.05$, or the corresponding energy loss of

$$\Delta_0 = \xi(\ln\frac{\xi}{\varepsilon'} + 0.37). \tag{7.8}$$

Δ_0 is called the most probable energy loss.

Although a detailed result of the inverse Laplace transforms of (7.4) indicated by Landau exists,[12] a simple result derived approximately by the saddle point method as shown in Fig. 9 will be also useful, explicitly represented by the variable λ:

$$\phi(\lambda)d\lambda = \frac{d\lambda}{\sqrt{2\pi e}}\exp[-\frac{\lambda}{2} - \exp(-\lambda-1)]. \tag{7.9}$$

8. Energy Loss Distribution Translated from the Excess-Path-Length Distribution

If we assume continuous ionization losses, the excess-path-length distribution is regarded as the energy-loss distribution. We compare it with the Landau distribution which is based on the statistical fluctuation of the collision energy loss. Although the latter is the dominant factor of the process the additional correction due to the excess-path-length distribution becomes serious with an increase of path length, because the width of collision-loss fluctuation increases proportional to the traversed thickness of material while that of the excess path length increases proportional to the square of the traversed thickness.

If we take ε as the constant energy loss per unit radiation length, then the width of the energy-loss distribution due to the multiple scattering evaluated from (3.2) is

$$\varepsilon\Gamma_A = 0.423\varepsilon\frac{2t^2}{w^2}. \tag{8.1}$$

ε is called the critical energy and usually used in the shower theory.[3] On the other hand, the width due to the collision loss fluctuation is[6]

$$\Gamma_L = 3.98\xi, \tag{8.2}$$

where ξ is a measure of the thickness defined in Eq. (7.6), rewritten as

$$\xi = \frac{0.154X_0\mathrm{MeVcm}^2}{\beta^2\Sigma A/\Sigma Z}t, \tag{8.3}$$

and X_0 and β denote the radiation length[3] and v/c, respectively.

If we measure the thickness of material in units of p^2c^2/E_s^2 and introduce a nondimensional thickness q,

$$q \equiv t/(pc/E_s)^2, \tag{8.4}$$

then the ratio of the former width to the latter becomes proportional to q:

$$\varepsilon\Gamma_A/\Gamma_L = \frac{\varepsilon\Sigma A/\Sigma Z}{2.90X_0\mathrm{MeVcm}^2}q. \tag{8.5}$$

The coefficient of q at the right-hand side is nearly 1, as indicated in Table IV, so we could use q as a parameter to approximately represent the correction ratio due to the excess-path-length distribution on the width of energy-loss distribution due to the collision-loss fluctuation.

TABLE IV. The coefficient against $t/(pc/E_s)^2$ in Eq. (8.5). The values of A and ε were taken from Ref. 44, and the compound rate of Nuclear Emulsion was taken from Ref. 55.

Material	Z	A	$\frac{\varepsilon \Sigma A/\Sigma Z}{2.90 X_0 \mathrm{MeV cm^2}}$
H	1	1.008	1.94
He	2	4.003	1.85
Li	3	6.940	1.32
C	6	12.010	1.26
N	7	14.008	1.52
O	8	16.000	1.50
Al	13	26.980	1.18
Si	14	28.090	1.17
Fe	26	55.85	1.10
Cu	29	63.54	1.09
Br	35	79.916	1.08
Ag	47	107.868	1.05
I	53	126.910	1.04
W	74	183.92	1.02
Pb	82	207.21	1.01
Compound Materials			
Air			1.51
SiO_2			1.19
H_2O			1.25
L_iH			1.35
Nuclear Emulsion			1.09

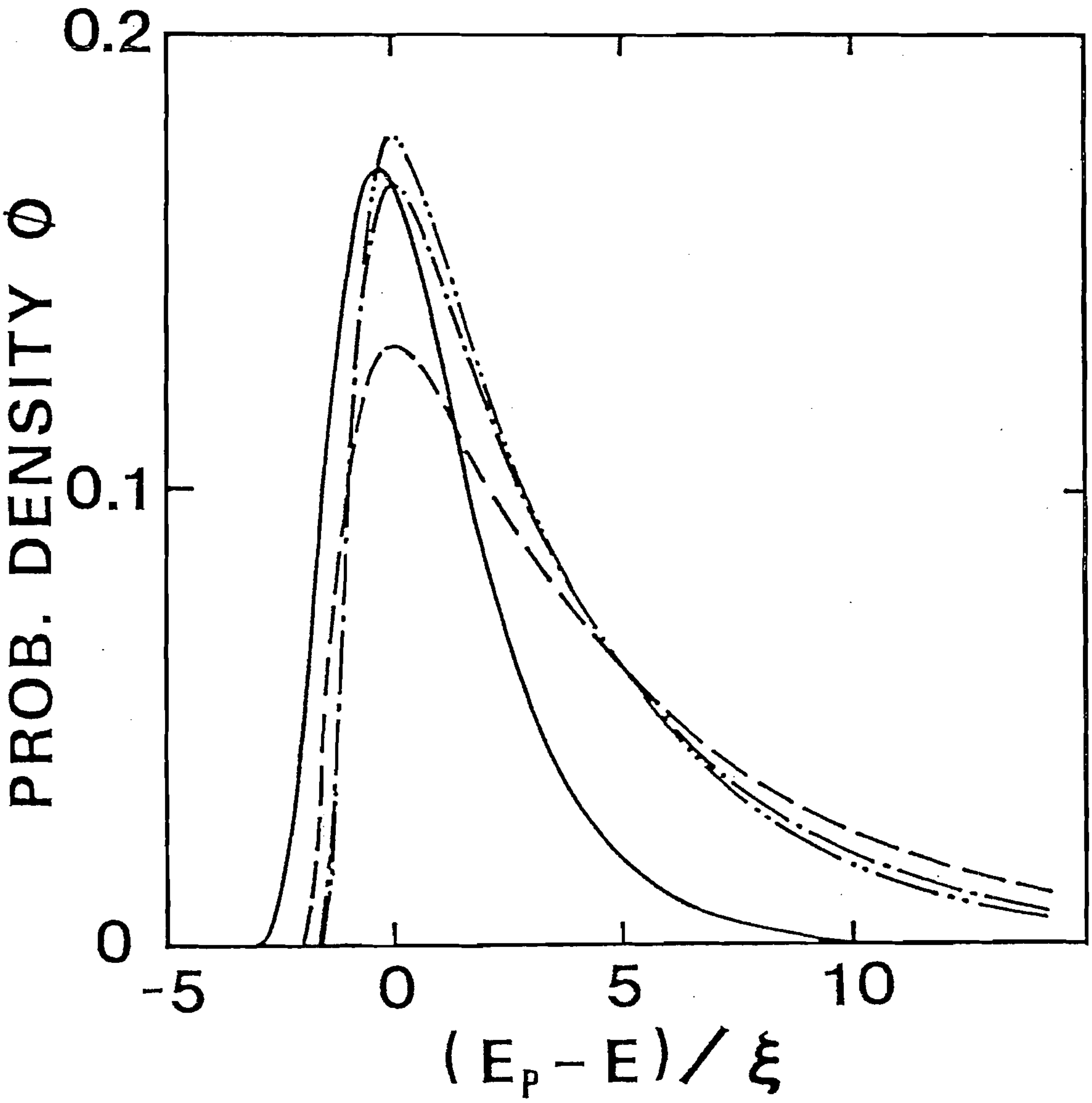

Fig. 9. An energy-loss distribution translated from the excess-path-length distribution with an assumption of continuous energy loss at a thickness of $t/(pc/E_s)^2=1$ in N (dashed curve), Al (dot-dashed curve), and Pb (double-dot-dashed curve), compared with that evaluated by the statistical fluctuation of collision loss predicted by Landau (solid curve). The width of the former increases proportional to the square of the thickness, while the width of the latter increases proportional to the thickness. Abscissa is energy loss in the unit of ξ defined by Landau.

The ratio of the mean excess path length to the thickness can be evaluated as

$$\langle \Delta_l \rangle_{av}/t = q/(4\beta^2), \tag{8.6}$$

so that we see the correction factor due to the excess-path-length distribution for the width of energy-loss distribution is about four times greater than that for the most probable energy loss.[56]

The excess-path-length distributions of case I translated to the energy-loss distribution assuming the continuous energy loss are plotted in Fig. 9 against the variable of

$$\lambda = \varepsilon(\Delta-\Delta_p)/\xi = \frac{\varepsilon\Sigma A/\Sigma Z}{0.308X_0\mathrm{MeVcm^2}} q(u-\tfrac{1}{6}), \tag{8.7}$$

for N, Al, and Pb at q=1, and are compared with the approximated expression, Eq. (7.9), of the Landau distribution. Toward a smaller energy-loss region of the peak, the Landau distribution rapidly decreases, but it has a meaningless long tail reaching to $-\infty$ of λ. On the other hand, the former decreases more rapidly and falls to zero corresponding to the fact that there is no excess of the path, irrespective of using the saddle-point method. Toward the large energy-loss region both distributions decrease exponentially, but the former decreases twice as slowly as the latter distribution. Thus multiple scattering gives a large contribution than the Landau distribution in the high-energy-loss region.

9. Experimental Survey

We see the typical elongation caused by the multiple scattering in the data of Hungerford and Birkhoff[22] [passage of 624 keV electrons through 54.5 mg/cm² Al (q=0.96), Fig. 10], and

McDonell, Hanson, and Wilson[28] [1 MeV electrons through 156 mg/cm^2 Al (q=1.4), Fig. 11], although in those experiments through the thinner material, we see good agreement with the Landau distribution; through 15.1 mg/cm^2 Al (q=0.27) in the former and through thickness less than the critical thickness, 50 mg/cm^2 Al (q=0.45), in the latter.

In experiments through gaseous matter with q less than 0.1 (Ref. 23, Fig. 12), we see good agreement with the Landau distribution at the tail of the distribution. In the experiments of high-energy electrons with q less than 0.3, the results agree well with the Landau distribution after taking account of polarization effects,[6,29] as indicated in Fig. 13. For heavier particles, by cosmic-ray muons with q of order of 10^{-4} (Refs. 30 and 31, Figs. 14 and 15) and by proton with q of order of 10^{-5} and 10^{-6} (Ref. 32, Fig. 16) the results agree well with the Landau distribution.

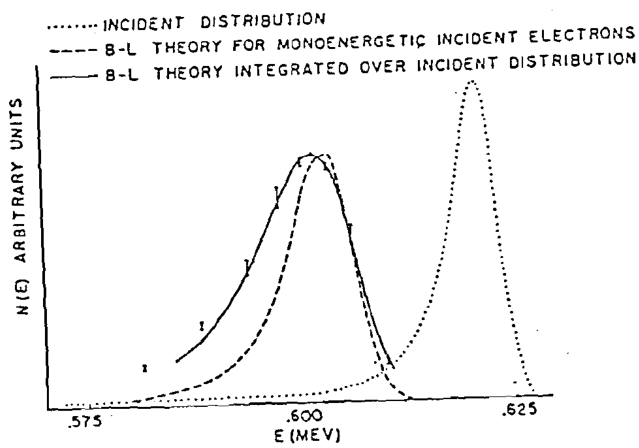

FIG. . Theoretical and experimental straggling distributions for 15.1 mg/cm² aluminum foil.

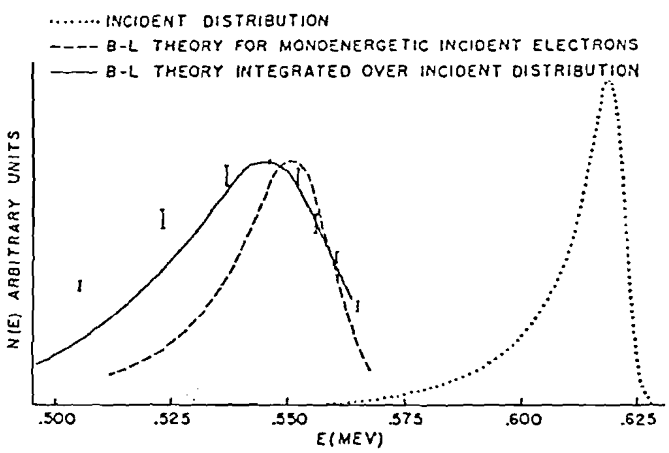

FIG. . Theoretical and experimental straggling distributions for 54.5 mg/cm² aluminum foil.

Fig. 10 The data of Hungerford and Birkhoff, cited from Ref. 22.

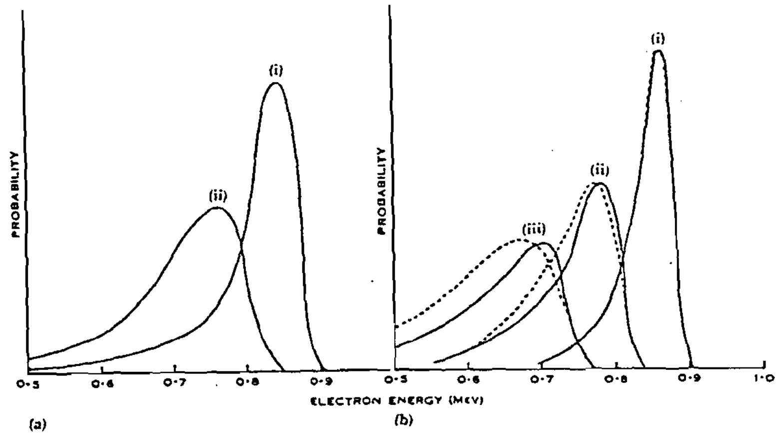

Fig. —Energy distributions of 1 MeV electrons after passing through aluminium; (i) 105 mg/cm², (ii) 158 mg/cm², (iii) 210 mg/cm². (a) Monte Carlo (Rossi-Greisen theory) distribution. (b) Full curve: Monte Carlo (Molière theory) distribution. Dashed curve: folded (Landau, modified Yang) distribution.

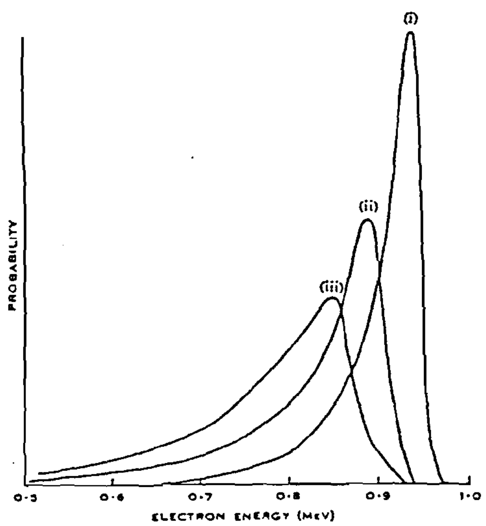

Fig. —Energy distribution of 1 MeV electrons after passing through gold: Monte Carlo (Molière theory); (i) 73 mg/cm², (ii) 110 mg/cm², (iii) 147 mg/cm².

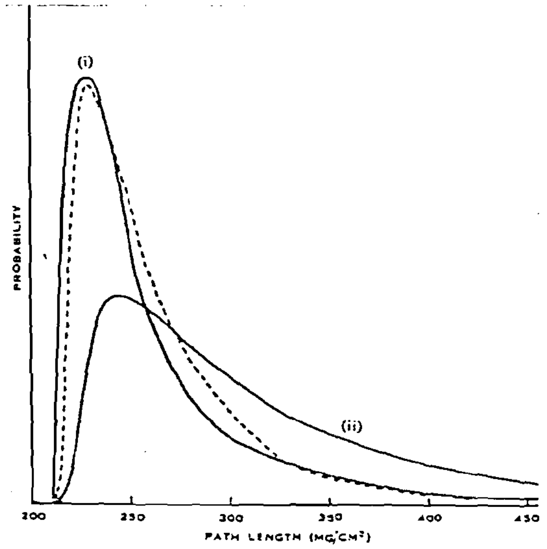

Fig. —Path length distribution of 1 MeV electrons incident normally on 210 mg/cm² of aluminium. (i) Full curve: Monte Carlo (Molière theory) distribution. Dashed curve: modified Yang distribution. (ii) Unmodified Yang distribution.

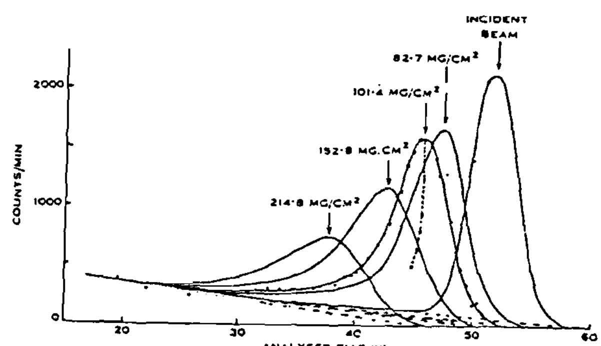

Fig. —Results of one experimental run. The scatter of the points about the estimated smooth curve is shown in one case. The points —×—×— are those used to determine the position of the peak, as described in the text.

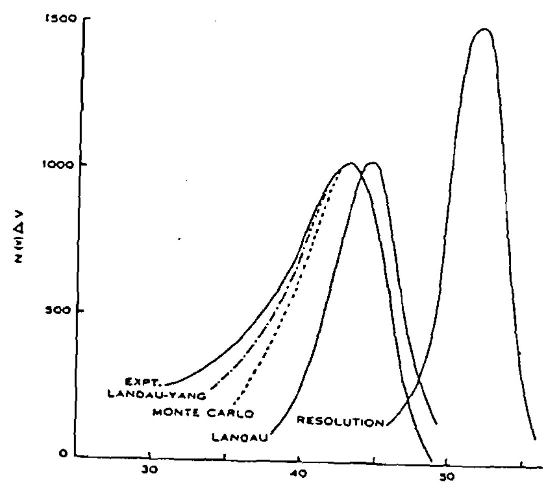

Fig. —Experimental distribution compared with theoretical curves folded with resolution curve.

Fig. 11 The data of McDonell, Hanson, and Wilson, cited from Ref. 28.

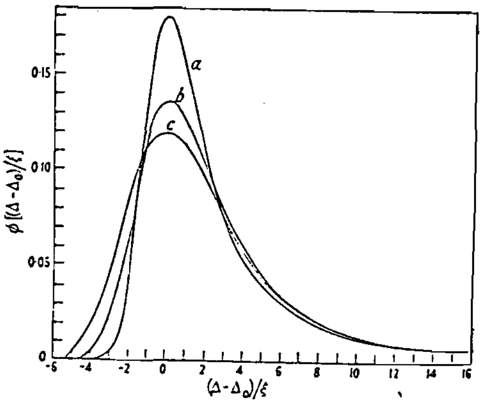

Figure . Energy-loss distributions for minimum ionizing electrons: curve *a*, theoretical distribution according to Landau; curve *b*, average experimental distribution in argon; curve *c*, average experimental distribution in krypton.

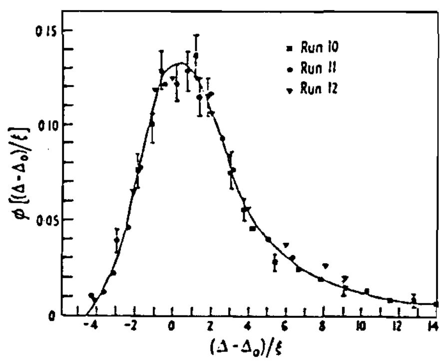

Figure Energy-loss distribution for minimum ionizing electrons in argon.

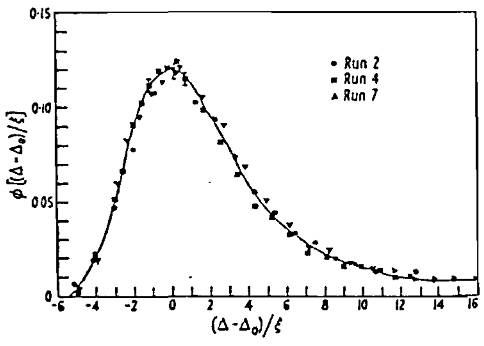

Figure · Energy-loss distribution for minimum ionizing electrons in krypton.

Fig. 12 The data of Rothwell, cited from Ref. 23.

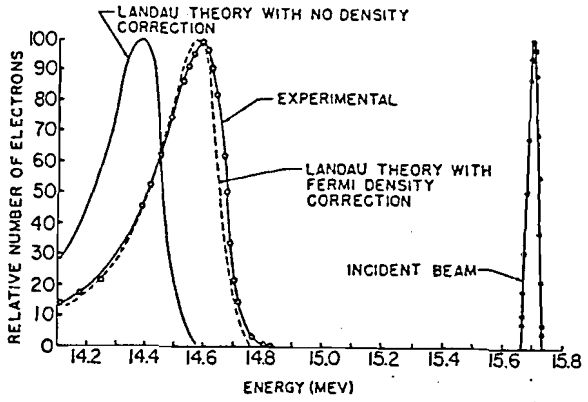

FIG. . Energy distribution of unobstructed electron beam and calculated and experimental distributions of electrons after passing through 0.86 g/cm² of aluminum.

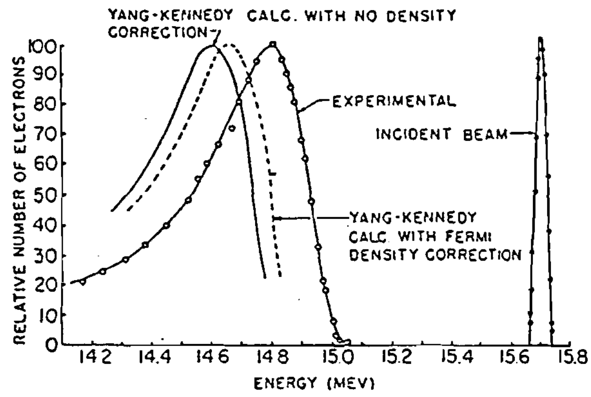

FIG. · Energy distribution of unobstructed electron beam and calculated and experimental distributions of electrons after passing through 0.97 g/cm² of gold.

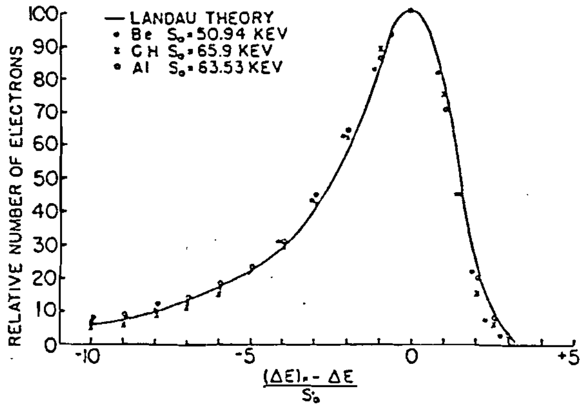

FIG. . Calculated and experimental straggling distributions of 15.7-Mev electrons after passing through absorbers of about 1 g/cm² of beryllium, polystyrene, and aluminum plotted *versus* energy in units of $S_0=2\pi e^4nl/mv^2$.

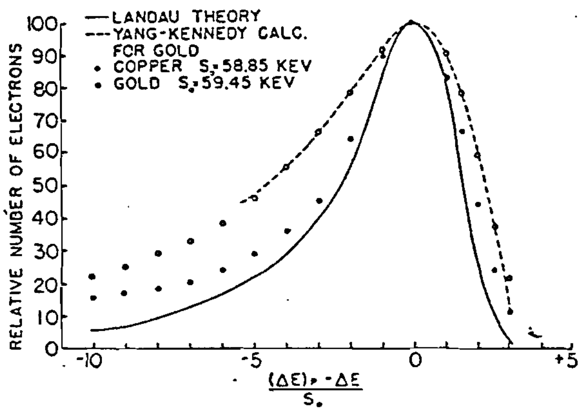

FIG. . Calculated and experimental straggling distributions of 15.7-Mev electrons after passing through absorbers of about 1 g/cm² of copper and gold plotted *versus* energy in units of $S_0=2\pi e^4nl/mv^2$.

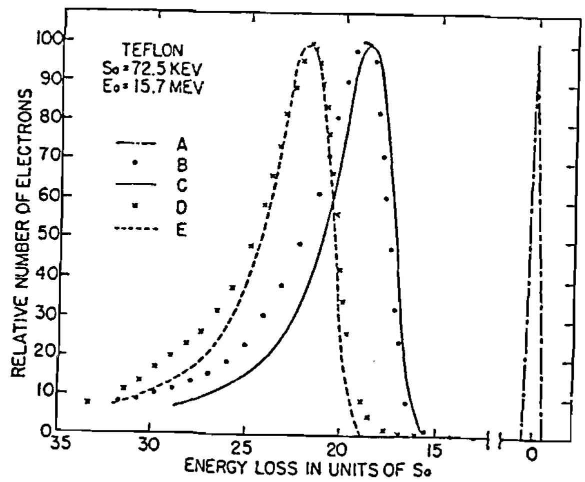

FIG. . Energy distributions of: (A) unobstructed electron beam; (B) experimental points for solid Teflon; (C) theoretical prediction for solid; (D) experimental points for Teflon's gaseous monomer; (E) theoretical prediction for gas.

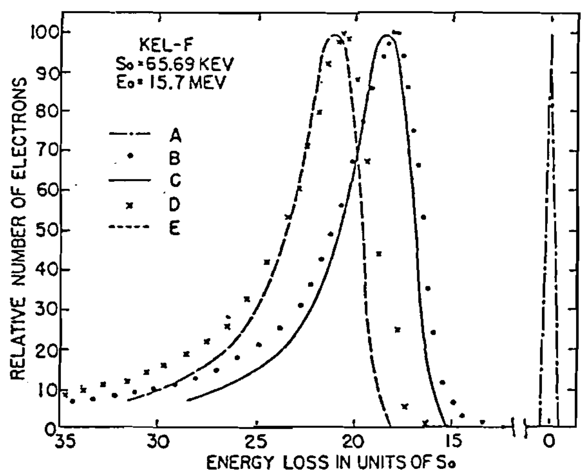

FIG. · Energy distributions of: (A) unobstructed electron beam; (B) experimental points for solid Kel-F; (C) theoretical prediction for solid; (D) experimental points for Kel-F's gaseous monomer; (E) theoretical prediction for gas.

Fig. 13 The data of Goldwasser, Mills, Hanson, and Robillard, cited from Refs. 6 and 29.

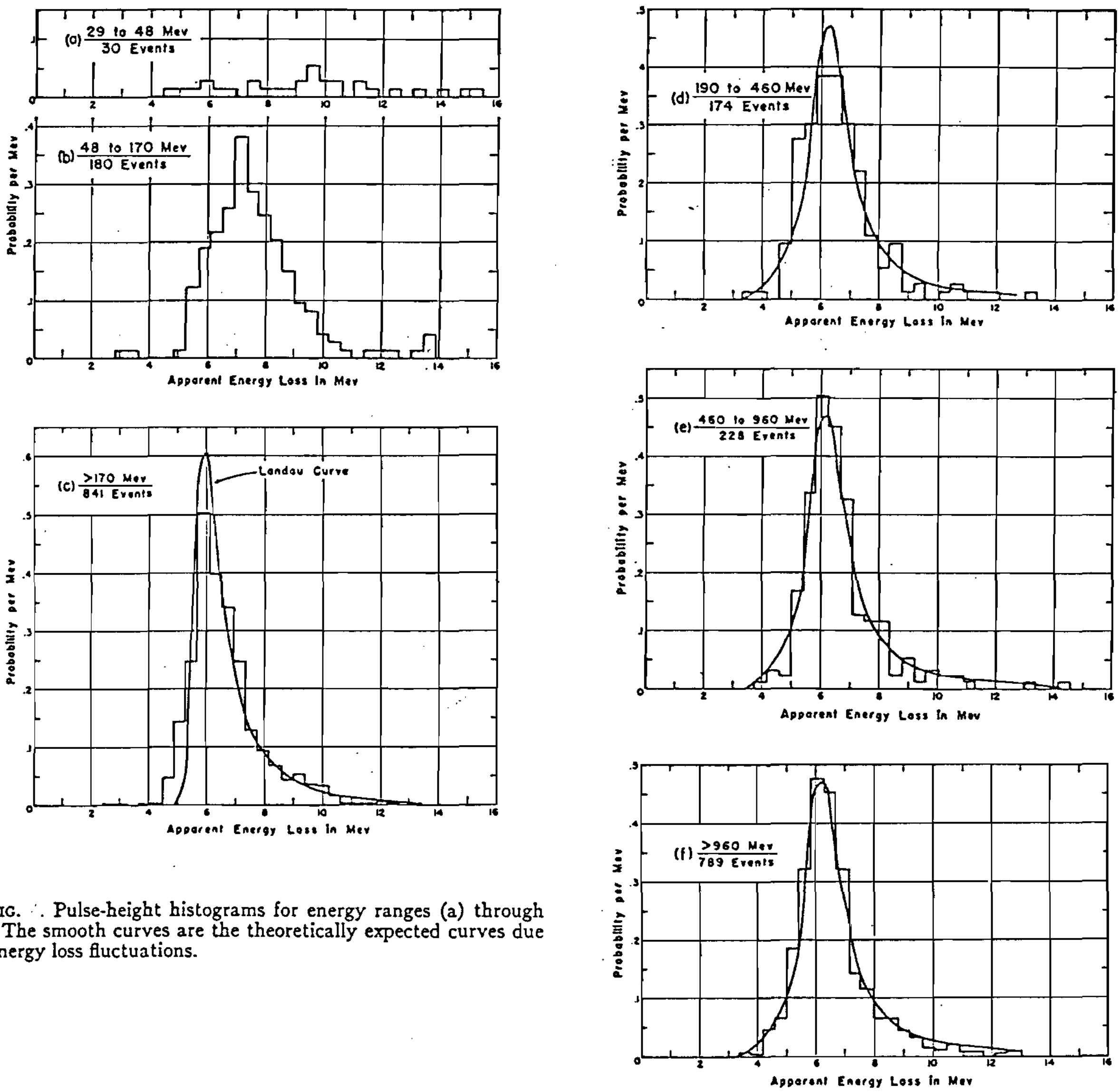

FIG. . Pulse-height histograms for energy ranges (a) through (f). The smooth curves are the theoretically expected curves due to energy loss fluctuations.

Fig. 14 The data of Roser and Bowen, cited from Ref. 30.

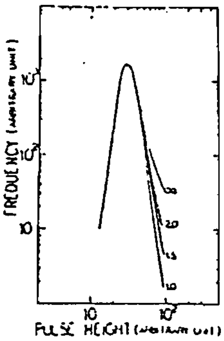

Fig.
Pulse height distributios (PMT R1084, 5 cm scintillator, n = 1.0, 1.5, 2.0, ∞)

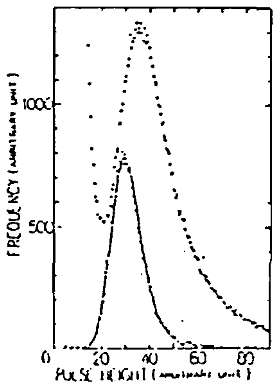

Fig.
Pulse height distribution (PMT R1084, 5 cm scintillator, n = 1.0)

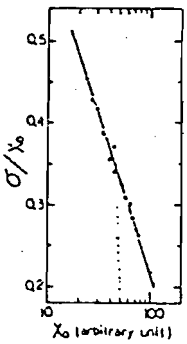

Fig.
Dispersion by the PMT effect

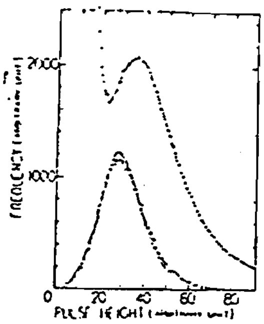

Fig.

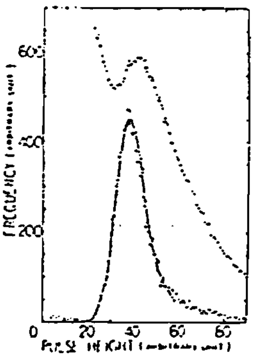

Fig.

Fig.
Pulse height distribution (PMT 6342A, 5 cm scintillator, n = 1.5)

Fig.
Pulse height distribution (PMT R1084, 0.3 cm scintillator, n = 1.5)

Fig. 15 The data of Hata, Asakimori, Maeda, Toyoda, Yoshida, and Kameda, cited from Ref. 31.

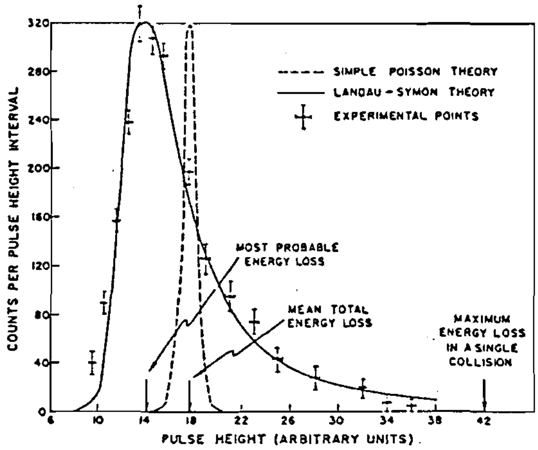

FIG. Frequency distribution of energy losses of 37-Mev protons traversing a 10-cm argon proportional counter at a pressure of 0.2 atmos. The theoretical distribution is calculated from the formulas of Symon (reference 3). The dashed curve is a Poisson distribution based on the statistics of the number of ion pairs formed in track.

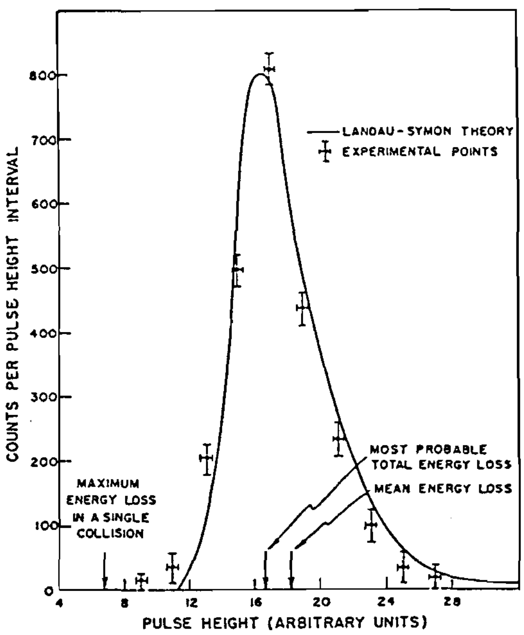

FIG. Frequency distribution of energy losses of 37-Mev protons traversing a 10-cm argon proportional counter at a pressure of 1.2 atmos.

Fig. 16 The data of Gooding and Eisberg, cited from Ref. 32.

V. CONCLUSIONS AND REMARKS

The excess-path-length distribution of fast charged particles due to multiple Coulomb scattering is completely solved in the Laplace transformed form under the small-angle and the Gaussian approximations following Yang's method (Table II). And the inverse Laplace transforms can be obtained to sufficient accuracy by the rapidly converging series, up to case III in Table I, and to good accuracy by the saddle-point method for general cases (in Table I and in Figs. 1-4).

Effect of the single scattering on the path length problem is investigated following the Molière theory (in Figs. 5-8). It is reconfirmed that the solutions under the Gaussian approximation are still a good first approximation under the more advanced Molière theory. But a distinctive long tail appears corresponding to the geometrical excess by the single scattering, and the distribution increases slightly in the small excess region, especially in the case of small thickness, which qualitatively agrees well with Molière's results for the angular distribution.

The energy-loss distribution translated from the excess-path-length distribution with an assumption of continuous energy loss is compared with that due to the collision-loss fluctuation. It is found that the ratio of correction due to the excess of path length on the width of the distribution, approximately represented by a new nondimensional thickness q of traversed material defined by (8.4), is about four times greater than that on the most probable energy loss [Eqs. (8.5) and (8.6), and Fig. 9].

In spite of the known defects mentioned above, the solutions of the excess-path-length distribution under the Gaussian approximation are important because of their completeness in mathematics and their relative convenience in handling, if enough care is taken for their limits.

ACKNOWLEDGMENTS

The author wishes to express his thanks to Professor Y.Toyoda, Professor Y.Tsuzuki, and Professor K.Kobayakawa for hearty instructions and advices at his preparation of this thesis. The daily discussions with Professor T.Kitamura, Doctor S.Dake, Doctor T.Maeda, Doctor T.Yanagita, Doctor K.Mizushima, Doctor K.Asakimori, Doctor N.Inoue, Mister K.Kihara, Mister J.Iyono, and Mister K.Yamaoka were very much valuable. He would like to thank Professor N.Ogita, Professor G.Tanahashi, Professor A.Misaki, Professor T.Sugihara, Professor H.Sasaki, Professor Y.Minorikawa, Professor M.Hazama, Doctor S.Kino, Doctor Y.Hatano, Doctor S.Tanaka, and Doctor J.Iwai, as well as the coworkers of the Norikura air-shower group for many useful comments to this work, and Professor K.Watanabe for the discussions about the mathematical contents. He is very much grateful to Professor R.W.Clay, Professor X.Gao, Professor A.M.Hillas, and Professor J.Linsley for giving him many advices and introducing him relating problems to this work. He also thanks to Professor H.Bichsel, Doctor H.Dai, Professor T.K.Gaisser, Professor H.Hasegawa, Professor G.B.Khristiansen, Professor J.Navarra, Professor M.V.S.Rao, Professor O.Saavedra, Professor K.Suga, Professor T.Wada, Doctor I.Yamamoto, for useful discussions about the work. The author wishes to express his special thanks to Professor C.N.Yang, who was the proposer of this problem, for giving him heartful messages and indicating much interest to the work. That was the highest encouragement to him through the work.

APPENDIX A: GENERALIZED GENERATING FUNCTION OF THE EIGENFUNCTION

The summation is obtained by using various levels of the generating functions with hermite polynomials, written as

$$H_{2m}(x) = (-1)^m (2m)! \sum_{k=0}^{m} \frac{1}{(2k)!(m-k)!} (-4x^2)^k, \tag{A1}$$

$$H_{2m+1}(x) = (-1)^m (2m+1)! 2x \sum_{k=0}^{m} \frac{1}{(2k+1)!(m-k)!} (-4x^2)^k. \tag{A2}$$

We use the following generating functions:

$$\sum_{m=0}^{\infty} \frac{1}{m!} t^m H_{2m}(x) = (1+4t)^{-\frac{1}{2}} \exp(\frac{4x^2 t}{1+4t}), \tag{A3}$$

$$\sum_{m=0}^{\infty} \frac{1}{m!} t^m H_{2m+1}(x) = 2x(1+4t)^{-\frac{3}{2}} \exp(\frac{4x^2 t}{1+4t}), \tag{A4}$$

$$\sum_{m=k}^{\infty} \frac{1}{(m-k)!} t^{m-k} H_{2m}(x) = (1+4t)^{-k-\frac{1}{2}} H_{2k}(\frac{x}{\sqrt{1+4t}}) \exp(\frac{4x^2 t}{1+4t}), \tag{A5}$$

$$\sum_{m=k}^{\infty} \frac{1}{(m-k)!} t^{m-k} H_{2m+1}(x) = (1+4t)^{-k-1} H_{2k+1}(\frac{x}{\sqrt{1+4t}}) \exp(\frac{4x^2 t}{1+4t}), \tag{A6}$$

or to be summarized as

$$\sum_{m=0}^{\infty} \frac{1}{m!} t^m H_{2m+k}(x) = (1+4t)^{-\frac{1}{2}(k+1)} H_k(\frac{x}{\sqrt{1+4t}}) \exp(\frac{4x^2 t}{1+4t}). \tag{A7}$$

Equations (A3) and (A4) can be derived by binomial series. Equations (A5) and (A6) are derivatives of (A3) and (A4), respectively, and can be proved by the mathematical induction method, or directly proved using the Laplace transforms and the formula

$$\frac{d^m}{dt^m}[\frac{1}{\sqrt{\pi t}} \exp(-\frac{k^2}{4t})] = L^{-1}[s^{m-\frac{1}{2}} \exp(-k\sqrt{s})]$$

$$= (4^m t^m \sqrt{\pi t})^{-1} H_{2m}(\frac{k}{2\sqrt{t}}) \exp(-\frac{k^2}{4t}). \tag{A8}$$

Then

$$\sum_{m=0}^{\infty} \frac{1}{(2m)!} H_{2m}(x) H_{2m}(y) (\frac{z}{2})^{2m}$$

$$= \sum_{m=0}^{\infty} \frac{1}{(2m)!} H_{2m}(x) (\frac{z}{2})^{2m} (-1)^m (2m)! \sum_{k=0}^{\infty} \frac{1}{(2k)!(m-k)!} (-4y^2)^k$$

$$= \sum_{k=0}^{\infty} \frac{1}{(2k)!} (-4y^2)^k \sum_{m=k}^{\infty} \frac{1}{(m-k)!} (-\frac{z^2}{4})^m H_{2m}(x)$$

$$= \frac{1}{\sqrt{1-z^2}} \exp\left(-\frac{z^2x^2}{1-z^2}\right) \sum_{k=0}^{\infty} \frac{1}{(2k)!} (-4y^2)^k \left(-\frac{z^2}{4}\right)^k (1-z^2)^{-k} H_{2k}\left(\frac{x}{\sqrt{1-z^2}}\right)$$

$$= \frac{1}{\sqrt{1-z^2}} \exp\left(-\frac{x^2+y^2}{1-z^2} z^2\right) \mathrm{ch}\left(\frac{2xyz}{1-z^2}\right). \tag{A9}$$

Similarly

$$\sum_{m=0}^{\infty} \frac{1}{(2m+1)!} H_{2m+1}(x) H_{2m+1}(y) \left(\frac{z}{2}\right)^{2m+1}$$

$$= \frac{1}{\sqrt{1-z^2}} \exp\left(-\frac{x^2+y^2}{1-z^2} z^2\right) \mathrm{sh}\left(\frac{2xyz}{1-z^2}\right). \tag{A10}$$

Thus we obtain

$$\sum_{n=0}^{\infty} \frac{1}{n!} H_n(x) H_n(y) \left(\frac{z}{2}\right)^n = \frac{1}{\sqrt{1-z^2}} \exp\left[-\frac{(x^2+y^2)z^2-2xyz}{1-z^2}\right], \tag{A11}$$

known as Mehler's formula.[57] Hence

$$\sum_{n=0}^{\infty} \psi_n(x) \psi_n(y) z^n = \frac{1}{\sqrt{\pi}\sqrt{1-z^2}} \exp\left[-\frac{(x^2+y^2)(1+z^2)-4xyz}{2(1-z^2)}\right]. \tag{A12}$$

APPENDIX B: AN EXAMPLE OF CALCULATING LOGARITHMIC DERIVATIVES OF LAPLACE TRANSFORMED SOLUTION

We indicate a sample method to obtain the logarithmic derivatives of $\Xi(s)$, for case V:

$$\Xi_V(s) = \frac{1}{3\pi} \frac{s^{3/2}}{\sqrt{s}\,\mathrm{ch}\sqrt{s}-\mathrm{sh}\sqrt{s}} \exp\left[-\frac{\rho^2}{3} \frac{s^{3/2}\mathrm{ch}\sqrt{s}}{\sqrt{s}\,\mathrm{ch}\sqrt{s}-\mathrm{sh}\sqrt{s}}\right]. \tag{B1}$$

Putting

$$f(x) = x\,\mathrm{ch}x - \mathrm{sh}x \quad \text{where} \quad x = \sqrt{s}, \tag{B2}$$

then

$$f'(x) = x\,\mathrm{sh}x, \qquad f''(x) = x\,\mathrm{ch}x + \mathrm{sh}x \tag{B3}$$

and so on. And if we put

$$\ln f(x) = g(x) \quad \text{and} \quad \ln \Xi(s) = L(x), \tag{B4}$$

then

$$L(x) = -\ln(3\pi) + 3\ln x - g - \frac{\rho^2}{6} x^2 (1+g''+g'^2), \tag{B5}$$

$$L'(x) = \frac{3}{x} - g' - \frac{\rho^2}{6} [x^2(g^{(3)}+2g'g'') + 2x(1+g''+g'^2)], \tag{B6}$$

$$L''(x) = -\frac{3}{x^2} - g'' - \frac{\rho^2}{6}[x^2(g^{(4)}+2g'g^{(3)}+2g''^2)$$

$$+4x(g^{(3)}+2g'g'')+2(1+g''+g'^2)]. \quad \text{(B7)}$$

Thus we obtain

$$\frac{d}{ds}\ln\Xi(s) = \frac{1}{2x}L'(x), \quad \text{(B8)}$$

$$\frac{d^2}{ds^2}\ln\Xi(s) = \frac{1}{4x^2}L''(x) - \frac{1}{4x^3}L'(x). \quad \text{(B9)}$$

The logarithmic derivatives for other cases can also be obtained by the same method.

APPENDIX C: PHYSICAL RESTRICTION CORRESPONDING TO THE GAUSSIAN APPROXIMATION IN MULTIPLE-SCATTERING THEORY

The angular distribution of fast charged particles due to multiple scattering is determined from stochastic superposition of Rutherford single scattering:[58]

$$\sigma(\theta)2\pi\theta d\theta dx = \frac{1}{2\ln(183Z^{-1/3})}\frac{E_s^2}{p^2v^2}\frac{d\theta}{\theta^3}dt. \quad \text{(C1)}$$

After passing through material of thickness x, the angular distribution represented by the nondimensional angle ϕ becomes

$$f(x,\vec{\theta})d\vec{\theta}$$

$$= \frac{d\vec{\theta}}{2\pi}\int_0^\infty \zeta d\zeta J_0(\zeta\theta)\exp[-x\int_{\theta_{min}}^{\theta_{max}}\{1-J_0(\zeta\theta')\}\sigma(\theta')2\pi\theta' d\theta']$$

$$= \frac{d\vec{\phi}}{2\pi}\int_0^\infty \alpha d\alpha J_0(\alpha\phi)\exp[-\frac{1}{2\ln(183Z^{-1/3})}\int_{\phi_{min}}^{\phi_{max}}\{1-J_0(\alpha\phi')\}\frac{d\phi'}{\phi'^3}], \quad \text{(C2)}$$

where we assumed the upper limit $\theta_{max} \sim \lambda\!\!\!^{-}/d \sim 100$ MeV/pc and the lower limit $\theta_{min} \sim \lambda\!\!\!^{-}/a \sim 0.01$ MeV/pc on the cross section corresponding to the radii of the nucleus and atom.[3]

If we develop $1-J_0(\alpha\phi')$ in power series, we get

$$f(x,\theta)d\vec{\theta}$$

$$= \frac{d\vec{\phi}}{2\pi}\int_0^\infty \alpha d\alpha J_0(\alpha\phi)\exp[-\frac{1}{4}M_2\alpha^2+\frac{1}{64}M_4\alpha^4-\frac{1}{2304}M_6\alpha^6+\ \ldots\ ], \qquad (C3)$$

where M_{2n} is the 2nth moment of the single scattering with ϕ at the depth x, and, as $\theta_{max}/\theta_{min} \sim 183^2Z^{-2/3}$ holds,[33]

$$M_2 = 1, \qquad (C4)$$

$$M_{2n} = \frac{1}{2n-2}\frac{1}{2\ln(183Z^{-1/3})}\phi_{max}^{2n-2}\{1-(\frac{\theta_{min}}{\theta_{max}})^{2n-2}\} \qquad (n>1). \qquad (C5)$$

If we can neglect the 4th moment and higher of M_{2n}, Eq. (C3) becomes the form derived from the Fokker-Planck approximation[46] and we get the simple Gaussian distribution

$$f(x,\theta)d\vec{\theta} = \frac{d\vec{\phi}}{\pi}e^{-\phi^2}. \qquad (C6)$$

This situation corresponds to the physical restriction of traversing a very large thickness, as

$$\phi_{max} = \theta_{max}/(\frac{E_s}{pv}\sqrt{t}) \ll 1, \quad \text{or} \quad t \gg 25. \qquad (C7)$$

It should also be noted that with an increase of t, integral range from ϕ_{min} to ϕ_{max} in (C2) becomes narrow and the value of the integrand increases; at the limit of $t\to\infty$ we reach the mathematical restriction against the Gaussian approximation shown by Nishimura [((A.3.11) in Ref.46)],

$$x\sigma(\theta)2\pi\theta d\theta = \lim_{\varepsilon\to 0}\frac{\delta(\phi-\varepsilon)}{\varepsilon^2}d\phi = \lim_{\delta\to 0}\frac{E_s^2t}{p^2v^2}\frac{\delta(\theta-\delta)}{\delta^2}d\theta. \qquad (C8)$$

APPENDIX D: THE KAMATA AND NISHIMURA FORMULATION OF THE MOLIÈRE THEORY AND ITS RELATION TO THE MOLIÈRE AND BETHE FORMULATION

Under the Molière theory we neglect the upper limit in the single scattering cross section ($\theta_{max}\to\infty$) and take the lower limit at $\sqrt{e}\chi_a$. Then the diffusion equation for the transformed angular distribution becomes

$$-d\ln\tilde{f} = dx\int_{\sqrt{e}\chi_a}^{\infty}\{1-J_0(\theta\zeta)\}\sigma(\theta)2\pi\theta d\theta. \tag{D1}$$

Kamata and Nishimura represented the Molière theory in differential form

$$-d\ln\tilde{f} = \frac{K^2\zeta^2}{4p^2v^2}\{1-\frac{1}{\Omega}\ln\frac{K^2\zeta^2}{4p^2v^2}\}dt, \tag{D2}$$

by introducing a new scattering energy K, almost identical with E_s, and a weight $1/\Omega$ indicating the magnitude of correction by the logarithmic term. K and Ω both are specific to the traversed material and independent of thickness t and momentum p. Introducing a new nondimensional variable and a complex variable,

$$\phi' = \frac{pv}{K\sqrt{t}}\theta \quad \text{and} \quad \alpha' = \frac{K\sqrt{t}}{pv}\zeta, \tag{D3}$$

then

$$\ln\tilde{f} = -\frac{\alpha'^2}{4}\{1-\frac{1}{\Omega}(\ln\frac{\alpha'^2}{4}-\ln t)\}, \tag{D4}$$

where the prime is attached to indicate that the value is defined from K instead of E_s.

In the Kamata and Nishimura formulation we can easily convert a diffusion equation from the Gaussian approximation to the Molière theory by only altering the term

$$\frac{E_s{}^2\zeta^2}{4p^2v^2} \quad \text{to} \quad \frac{K^2\zeta^2}{4p^2v^2}\{1-\frac{1}{\Omega}\ln\frac{K^2\zeta^2}{4p^2v^2}\}, \tag{D5}$$

but the explicit t in logarithm appears generally in the solution by this method due to an existence of lnt in (D4).

In the case of the angular distribution, Molière and Bethe originally introduced their weight and integration variables, 1/B and u (Ref. 59) which are slightly distinguished from $1/\Omega$ and α' by

$$B-\ln B = \Omega-\ln\Omega+\ln t \quad \text{and} \quad u = \frac{\sqrt{B}}{\sqrt{\Omega}}\alpha'. \tag{D6}$$

Then we get the Molière and Bethe formulation

$$\ln \tilde{f} = -\frac{u^2}{4}\{1-\frac{1}{B}\ln\frac{u^2}{4}\}, \tag{D7}$$

instead of (D4). Thus we can represent the angular distribution in a single nondimensional variable complementary to u:

$$\vartheta = \frac{\sqrt{\Omega}}{\sqrt{B}}\phi'. \tag{D8}$$

But in the path length problem under the Molière theory, the author could not find such a variable removing the explicit t.

APPENDIX E: CONTOUR INTEGRAL COMPRISING LOGARITHMIC PAIR

Let C be a contour on which f(ζ) is an analytic function of ζ and inside which f(ζ) has a finite number of poles. Then for all z inside the contour and on poles, we have[60]

$$\frac{1}{2\pi i}\int_C \frac{f(\zeta)}{\zeta-z}d\zeta = f(z)-\sum_{\mathrm{pole}}(\text{principal part}). \tag{E1}$$

Thus, integrating with z from α to β along any path inside the contour we get

$$\frac{1}{2\pi i}\int_C f(\zeta)\ln\frac{\zeta-\alpha}{\zeta-\beta}d\zeta = \int_\alpha^\beta \{f(\zeta)-\sum_{\mathrm{pole}}(\text{principal part})\}d\zeta. \tag{E2}$$

REFERENCES

1) W.T. Scott, Rev. Mod. Phys. 35, 231(1963).

2) C.N. Yang, Phys. Rev. 84, 599(1951). The Yang theory is also reviewed and discussed by Birkhoff in Ref.20.

3) B. Rossi and K. Greisen, Rev. Mod. Phys. 27, 240(1941).

4) E.J. Williams, Proc. R. Soc. London A169, 531(1939).

5) W.T. Scott, Phys. Rev. 75, 1763(1949).

6) E.L. Goldwasser, F.E. Mills, and A.O. Hanson, Phys. Rev. 88, 1137(1952).

7) C. Warner III and F. Rohrlich, Phys. Rev. 93, 406(1954).

8) D.V. Hebbard and P.R. Wilson, Aust. J. Phys. 8, 90(1955).

9) M.J. Berger, in "Methods in Computational Physics," edited by B. Adler, S. Fernbach, and M. Rotenberg (Academic, New York, 1962), Vol. I.

10) H. Bichsel and E.A. Uehling, Phys. Rev. 119, 1670(1960).

11) M. Messel and D.F. Crawford, "Electron-Photon Shower Distribution Function Tables for Lead Copper and Air Absorbers," (Pergamon, Oxford, 1970).

12) L. Landau, J. Phys. (U.S.S.R.) 8, 201(1944).

13) K.R. Symon, introduced by Rossi in Ref.33.

14) O. Blunck and S. Leisengang, Z. Phys. 128, 500(1950).

15) P.V. Vavilov, Zh. Eksp. Teor. Fiz. 32, 920(1957) [Sov. Phys. JETP 5, 749(1957)].

16) H. Bichsel, Phys. Rev. B1, 2854(1970).

17) E.J. Williams, Proc. R. Soc. London 125, 420(1929).

18) F. Kalil and R.D. Birkhoff, Phys. Rev. 91, 505(1953).

19) F. Rohrlich and B.C. Carlson, Phys. Rev. 93, 38(1954).

20) R.D. Birkhoff, in "Handbuch der Physik, Band 34," edited by S. Flügge (Springer, Berlin, 1958), p. 53.

21) R.D. Birkhoff, Phys. Rev. 82, 448(1951).

22) E.T. Hungerford and R.D. Birkhoff, Phys. Rev. 95, 6(1954).

23) P. Rothwell, Proc. Phys. Soc. London B64, 911(1951).

24) N.Hasebe et al., Nucl. Instr. Meth. 155, 491(1978).

25) Y.Iga et al., Nucl. Instr. Meth. 213, 531(1983).

26) J.J.L. Chen and S.D. Warshaw, Phys. Rev. 84, 355(1951).

27) S. Kageyama and K. Nishimura, J. Phys. Soc. Jpn., 7, 292(1952).

28) J.A. McDonell, M.A. Hanson, and P.R. Wilson, Aust. J. Phys. 8, 98(1955).

29) E.L. Goldwasser, F.E. Mills, and T.R. Robillard, Phys. Rev. 98, 1763(1955).

30) T. Bowen and F.X. Roser, Phys. Rev. 85, 992(1952).

31) T. Hata et al., "17th International Cosmic Ray Conference Paris, 1981, Conference Papers" (Centre d'Etudes Nuclaires, Saclay, 1981), Vol. 9, p.352.

32) T.J. Gooding and R.M. Eisberg, Phys. Rev. 105, 357(1957).

33) B. Rossi, "High Energy Particles" (Prentice-Hall, Englewood Cliffs, NJ, 1952).

34) R.R. Wilson, Phys. Rev. 84, 100(1951).

35) J. Linsley, J. Phys. G12, 51(1986).

36) P. Bassi, G. Clark, and B. Rossi, Phys. Rev. 92, 441(1953).

37) C. Aguirre et al., "16th International Cosmic Ray Conference, Kyoto, 1979, Conference Papers" (Institute of Cosmic Ray Research, University of Tokyo, Tokyo, 1979), Vol.8, p.112.

38) T. Nakatsuka, "18th International Cosmic Ray Conference,

Bangalore, India, 1983, Conference Papers," edited by N. Durgaprasad et al. (Tata Institute of Fundamental Research, Bombay, 1983), Vol. 11, p.29.

39) T. Nakatsuka, "Nineteenth International Cosmic Ray Conference, La Jolla, California, 1985," Contribution No. HE4.7-11 (late paper)(unpublished); Uchüsen-Kenkyu, 29, 167(1986).

40) L.V. Spencer, Phys. Rev. 84, 100(1951).

41) G. Molière, Z. Naturforsch. 3a,78(1948).

42) H.A. Bethe, Phys. Rev. 89, 1256(1953).

43) $\vec{\Delta}$ is not a vector. It only represents a set of Δ_y and Δ_z.

44) The equations, from (1.2) to (1.8), were derived by Yang and are cited from Ref.2. Except we used the Laplace transforms against Δ in (1.6) instead of the Fourier transforms, which made the expressions a little simpler and lead to the usage of the saddle-point method naturally at the inverse transforms.

45) "Handbook of Mathematical Functions with Formulas, Graphs, and Mathematical Tables," edited by M. Abramowitz and I.A. Stegun (Dover, New York, 1965), Chap.22.

46) J. Nishimura, in "Handbuch der Physik, Band 46," edited by S. Flügge (Springer, Berlin, 1967), Teil 2, p.1.

47) W.T. Scott, Phys. Rev. 76, 212(1949).

48) Infinitesimals up to the 15-th order with $\sqrt{s}$ appear in the numerator and the denominator in (2.8) and (2.9). The mean values and the variances are calculated using a symbolic and algebraic manipulating software REDUCE.

49) M.A. Locci, P. Picchi, and G. Verri, Nuovo Cimento 50B, 384(1967).

50) A.J. Baxter, J. Phys. A2, 50(1969).

51) G. Molière, Z. Naturforsch. 2a, 133(1947).

52) K. Kamata and J. Nishimura, Suppl. Prog. Theor. Phys. 6, 93(1958).

53) S.Hayakawa, Cosmic Ray Physics, New York: John Wiley & Sons(1969).

54) L.Livingstone and Bethe, Rev. Mod. Phys. 9, 245(1937).

55) T.H.Burnett et al., Phys. Rev. 35, 824(1987).

56) Similar discussion is made by Rohrlich and Carlson in Ref.19. They insisted the positron-electron difference in energy straggling appears more likely in the shape of the distribution than in the most probable energy loss.

57) A. Erdelyi et al., "Higher Transcendental Functions," (McGraw-Hill, New York, 1953), Vol. 2, Chap. 10. Actually, the author proved (A12) directly without using (A11). But the proof through Mehler's formula, here indicated, is equivalent and more transparent.

58) Comment on a confusion in an evaluation of the numeral 183 in (C1) is made by J. Linsley in "Proceedings of the Nineteenth International Cosmic Ray Conference, La Jolla, California, 1985," edited by F.C. Jones, J. Adams, and G.M. Mason (NASA Conf. Publ. No. 2376)(Goddard Space Flight Center, Greenbelt, MD, 1985), P.163.

59) This u defined by Bethe must not be confused with our u of (1.15).

60) E.T. Whittaker and G.N. Watson, "A course of modern analysis," 4th ed. (Cambridge University Press, Cambridge, England, 1965), Chap.5.